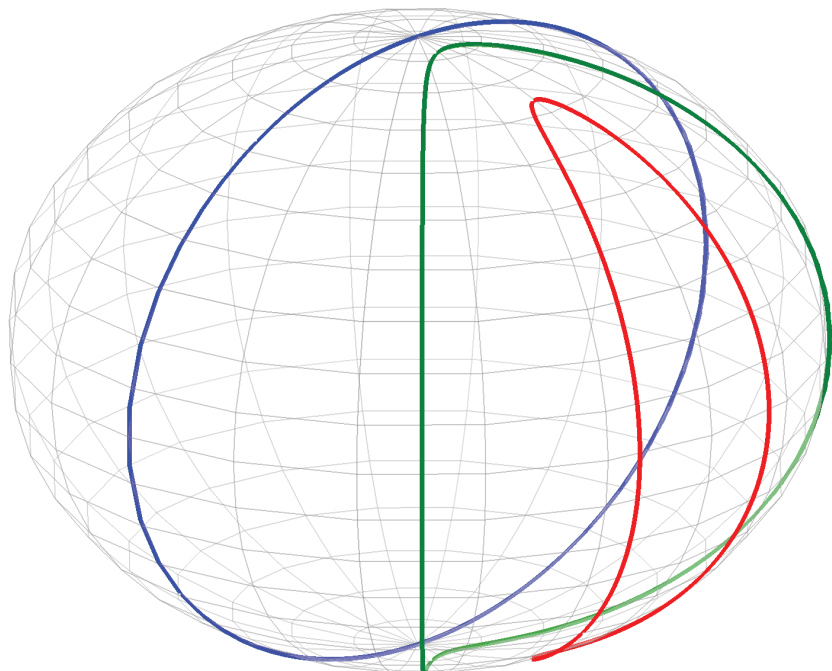
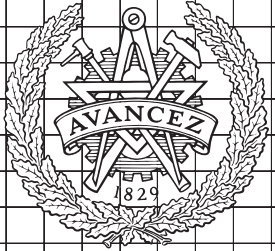


CHALMERS



Low Reynolds Number Particle Dynamics

Master's Thesis in Complex Adaptive Systems

JONAS EINARSSON

Department of Physics & Engineering Physics
Non-linear Dynamics & Statistical Physics
CHALMERS UNIVERSITY OF TECHNOLOGY
Gothenburg, Sweden 2011
Master's Thesis 2011:1

Abstract

The motion of rigid rod-like particles in a viscous microfluidic channel flow has been analyzed. We derive equations of motion from a 3-dimensional dumbbell model and show that they are equivalent to the well-known Jeffery equations. Experimental data shows a qualitative fit to the Jeffery theory, but we observe *orbit drift* indicating the presence of noise in the dynamics. Examples and numerical simulations of such dynamics are presented.

Future research prospects are presented in the form of a phase diagram to be explored. We propose that different theories describe the particle dynamics at high and low particle aspect ratio, as well as high and low noise levels.

A background chapter provides an introduction to the field of microhydrodynamics and briefly reviews the literature.

Acknowledgements

This thesis has been researched and written with supervision of Professor Bernhard Mehlig in the department of Physics at Gothenburg University. Thank you, Bernhard, for being ever enthusiastic regardless of how I do. It is fun to do physics here.

Dag Hanstorp and John Oladiran are the experimentalists who made these first movies available to us. Thanks for your patience with all my impossible requests. Thanks also go to the rest of Origo 7th floor staff for the hospitality shown, especially Stellan Östlund for help with SO3 numerical mysteries.

I'd also like to take the opportunity to thank Martin Cederwall for directing the undergraduate Physics programme at Chalmers during my years here. You always worked for our interests, and we worked like, quote, galley slaves. It was fun. Good luck with the new job.

Jonas Einarsson, Gothenburg January 25, 2011

Contents

1	Introduction	1
1.1	This thesis	1
1.2	Report disposition	2
1.3	Notation	2
1.4	Motivation	2
1.4.1	Particle transport	3
1.4.2	Rheoscopic visualizations and Poincaré indices	3
2	Background	6
2.1	Fluid dynamics	6
2.1.1	Flow basics and notation	6
2.1.2	Navier-Stokes	7
2.1.3	From Navier to Stokes	9
2.2	Hydrodynamics of particles	10
2.3	Rheology of suspensions	13
2.3.1	Viscosity	13
2.3.2	Einstein's 1906 result	14
2.4	Ellipsoid dynamics	14
2.4.1	The Jeffery orbits	16
2.4.2	Particle orientation distribution	16
2.4.3	Infinite aspect ratio models	17
3	Dynamics of rods	19
3.1	Experimental data	19
3.1.1	Movies	19
3.1.2	Analysis	20
3.2	Dumbbell model	22
3.2.1	Rotation matrix equation of motion	22
3.2.2	Finding the Jeffery equations	24
3.3	Dynamics of axisymmetric particles	25

3.3.1	Shear flow	28
3.3.2	Projection into Jeffery orbits	29
3.3.3	Experimental data	31
3.3.4	Possible perturbations	32
3.4	Conclusions & Outlook	37
3.4.1	Experiments	37
3.4.2	Theory	37
	Bibliography	42
A	Calculations & notes	43
A.1	Numerically integrating SO(3)	43
A.2	On the experimental fit	45
A.2.1	The method used	45
A.2.2	Attempt of improvement	45
A.3	Pressure driven flow in rectangular channel	48

1

Introduction

WHAT DO BLOOD and mayonnaise have in common? What is it about microchannels that make biochemists so very happy? And how did the department of theoretical physics get involved? As the title of this thesis implies it has got to do with particle dynamics. Small, micrometer-size and smaller still, particles exists everywhere. Living cells, macromolecules such as DNA and paper fibres are examples of micro sized particles. A common setting for these particles is to be suspended in some flow. For example a red blood cell in transit is a particle $6\text{--}8 \mu\text{m}$ suspended in the channel flow of a blood vessel.

The presence of suspended particles in a gas or liquid substantially changes the macroscopic properties of the latter. Pioneering work on this, as in many other fields, was done by Albert Einstein [1]. He calculated the increase in fluid viscosity due to suspended spherical particles. Mayonnaise is basically a suspension of oil droplets (particles) in water, its tasty thickness is due to particle motion dissipating energy.

The connection to the Life Sciences is not so difficult to imagine. Understanding of cell and protein motion is just one point. Biotechnology dreams of *Lab on a Chip*, devices to perform automated experimental measurements on microscale.

1.1 This thesis

What is this thesis about? In short: understanding the mechanisms behind the motion of solid particles suspended in fluids. For many reasons, which we shortly will return to, it is interesting to know the following: if we place a particle in a fluid, how will it behave? What is the trajectory, its orientation? How does it change with aspect ratio, what about noise? What happens if I put many particles in a fluid, making it a colloidal suspension?

This thesis is concerned with the matter of a single particle, moving in a fluid. The work is inspired by recent, and ongoing, experiments by Oladiran, Hanstorp and

1.2. REPORT DISPOSITION

Andersson[2]. They caught, on video, the time evolution of a rod-shaped particle's motion in a microchannel. Our aim is to model this motion, and deduce which interaction mechanisms are responsible for the observed behaviour. In particular we will revisit the theory of ellipsoids immersed in a viscous fluid first developed by Jeffery in 1922 [3]. His periodic solution of motion, the *Jeffery orbits*, will be the basis of our analysis.

1.2 Report disposition

This report is divided into three chapters. This first introductory chapter contains an explanation of the subject, requiring no prior knowledge. The aim is also to motivate this research and explain some reasons to investigate particle dynamics.

The second chapter is essentially a review of the large body of existing work. We will try to place this thesis in context, relate to neighbouring research and give a review of the most important publications that we build upon. This chapter may be partially or completely skipped by the reader already familiar with the subject. My intention is that a physics graduate student should be able to pick up what we have done, without any other specific prerequisites.

Chapter three deals with our own treatment of the subject. Specifically it describes recent experimental data and the efforts that went into modeling it.

1.3 Notation

As far as possible we explain notation as it is introduced. Table 1.1 lists a small set of standard symbols which are used without further explanation.

Table 1.1: Table of notation used in report

\mathbf{x}	Vector
$\hat{\mathbf{x}}$	Unit vector
A	Matrix
\dot{x}	Dot notation time derivative
\bar{z}	Complex conjugate

1.4 Motivation

The reason for initiating this research is two-fold. Most obvious is the study of transport of particles in an environment. With ever increasing precision researchers observe and manipulate small particles such as bacteria or single polymers. Such manipulation requires understanding of underlying behavior. The second and maybe more subtle reason for this project grew from recent research on rheoscopic fluids by Bezuglyy, Wilkinsson and Mehlig [4][5][6]. The remainder of this section discusses these two areas briefly.

1.4. MOTIVATION

1.4.1 Particle transport

The early investigators of particle dynamics could but dream of observing a micrometer object in motion, in real time. As in so many areas, technology have improved drastically and old theories resurface to explain observed phenomena. In biotechnology it is desirable to handle, sort and manipulate single molecules like proteins and DNA. Smith et al published a series of papers in Science on observations of single polymer dynamics in linear flows [7]. The experiments described in this report are ongoing research by Oladiran and Hanstorp [2]. Basically they observe, in real time, the motion of single polymer rods in a microchannel. We will return to the details in chapter 3, the point now is that we can finally test the theoretical results from early 20th century.

As one example of how the old theory resurfaces we will briefly describe an experiment published by Kaya and Koser in 2009 [8]. The bacterium *E.coli* is a rod-shaped cell, a few μm long and less than one μm wide. Kaya manufactured a microchannel and let a sample of bacteria sediment to the bottom. The channel was observed with a microscope while a pressure-driven flow advected the bacteria along the bottom surface. A schematic setup and resulting image is shown in figure 1.1. The result is analyzed in terms of the same Jeffery orbits we will discuss in this report. Kaya and Koser's observations make a strong case for the importance of research on the dynamics of micro and nano particles. We warmly recommend a visit to the online version of their paper¹ to view the supplemental video clips of *E.coli* flipping and kayaking.

1.4.2 Rheoscopic visualizations and Poincaré indices

On a more theoretical side, particle dynamics play a role in the topology of rheoscopic visualizations. Bezuglyy, Wilkinsson and Mehlig have published a series of papers on this subject [4][5][6].

A *rheoscopic* fluid is a suspension of microscopic rod-like particles. The name stems from its use in visualizing flow fields in experiments. Because the rods are anisotropic, the reflected light intensity from them has an angular dependence. Shining light with different colors from different directions gives information about the rod orientation, as the color is additive. An example of how this may look is shown in figure 1.2.

Intuitively one might believe that the rod particles will align with the flow lines, and that would be it. In reality there are subtle differences which lead to unexpected behavior. The authors argue that an incompressible, smooth flow would lead to a smooth vector field of particle orientation. However, judging from the picture in figure 1.2a there seems to be points where this is not the case.

Their analysis makes use of an idea from topology, the *Poincaré index*. Given a closed curve in a vector field, the index is simply the number of complete 2π rotations the vector makes as the curve is traversed once. There is an analogy to complex variables, where there are certain theorems regarding closed curve integrals and poles. For vector fields one theorem says that in a smooth vector field, any closed curve has Poincaré index 0. There are analogues to the theorem of continuous deformation of contours and in

¹<http://link.aps.org/doi/10.1103/PhysRevLett.103.138103>

1.4. MOTIVATION

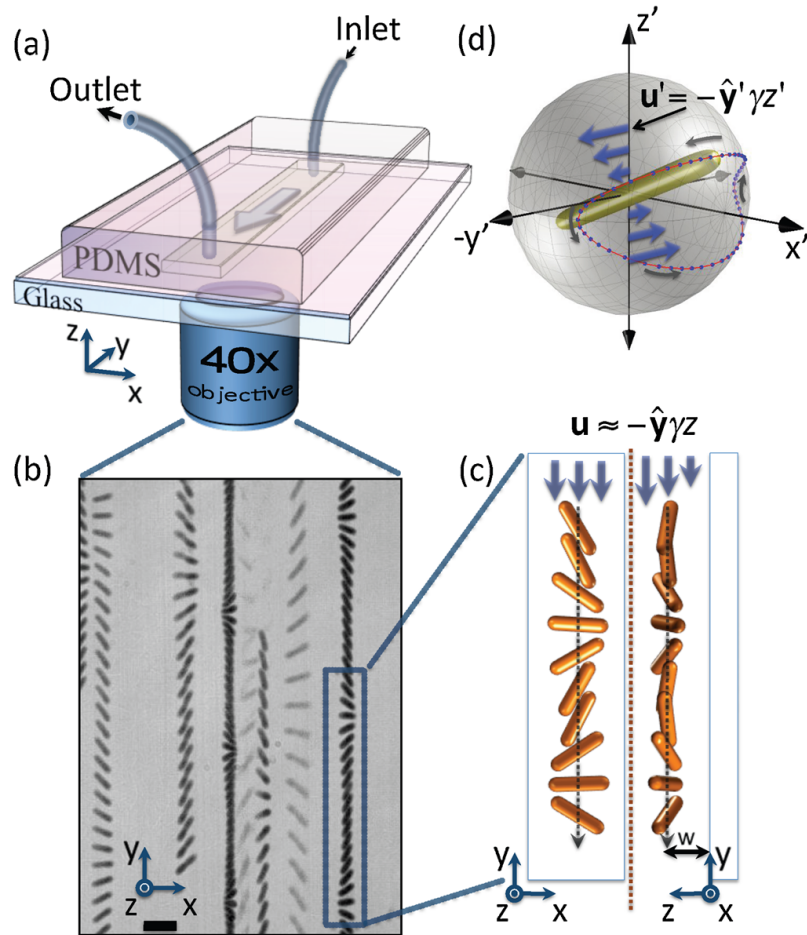
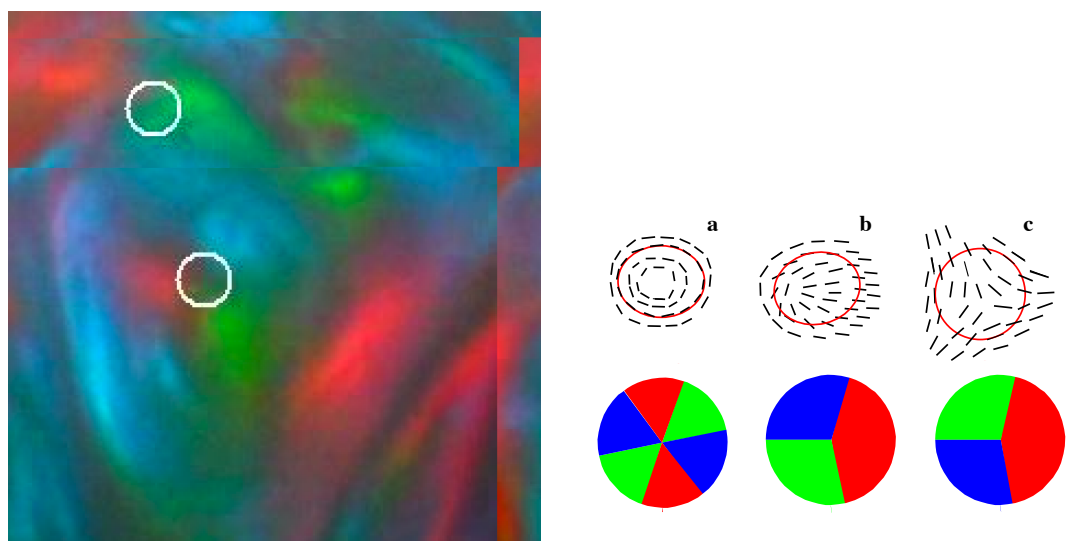


Figure 1.1: Experimental setup of Kaya and Koser [8]. A microchannel is observed from below using a microscope. The motion of *E.coli* bacteria is recorded on video and analyzed. Reproduced with permission from the authors.

particular the Poincaré index is related to the number of zeros enclosed by the contour. Note that the analogy is not perfect, and half-integer indices are allowed.

The basis of their calculations is the dynamical equations for a rod-like particle in a viscous flow. In the series of papers this is applied to various two-dimensional flow situations. It seems that the particles in most places behave as expected, but the alignment breaks down at certain points. These show up as singularities with non-zero Poincaré indices. It turns out exactly this kind of vector field singularity is used to characterize our fingerprints, hence the name of one paper “Fingerprints of random flows?”. A critical part in analyzing these vector fields is thorough understanding of the underlying particle dynamics.

1.4. MOTIVATION



(a) Rheoscopic liquid illuminated with three colors

(b) Singularities and corresponding color signature

Figure 1.2: Rheoscopic visualization with three colors. In the right figure the three cases correspond to a vortex with Poincaré index 1, and two other singularities with indices $\frac{1}{2}$ and $-\frac{1}{2}$, respectively.

2

Background

NEWTON IS CREDITED WITH the saying that we are standing on the shoulders of giants. Inevitably in a work like this, a large body of knowledge stands behind the results we can present. The intention is that a physics graduate student without prior experience in the field should be able to understand our work. To this end, this chapter contains assorted background knowledge, beginning with basic fluid dynamics, the reduction to Stokes flow and its application to particle hydrodynamics. A brief look into the wide field of Rheology follows before moving into a review of the Einstein and Jeffery results of single suspended particles. Several branches of research following Jeffery extends the theory with noise and other interactions to better explain experimental evidence.

2.1 Fluid dynamics

A just treatment of fluid dynamics is severely out of scope in this report. However, we want to review some key concepts so that the reader without experience with the subject will have an idea. In particular it is important to think about the many assumptions that leads to the linear Stokes equations for low Reynolds number flow, starting with the infamously non-linear Navier-Stokes equations. This section builds loosely on Kundu's book on fluid mechanics [9] and Brenner's volume on Low Reynolds number hydrodynamics [10].

2.1.1 Flow basics and notation

A *flow* in a fluid is specified by a flow velocity field $\mathbf{u}(\mathbf{r},t)$ and a pressure field $p(\mathbf{r},t)$. Any flow $\mathbf{u}(\mathbf{r})$ can be locally linearized by the first order Taylor expansion around an

2.1. FLUID DYNAMICS

arbitrary point \mathbf{r}_0

$$\mathbf{u}(\mathbf{r}) \approx \mathbf{u}(\mathbf{r}_0) + \underbrace{\frac{d\mathbf{u}}{d\mathbf{r}}}_{A} (\mathbf{r} - \mathbf{r}_0)$$

It is convenient to express the flow Jacobian A in its symmetric and antisymmetric parts and write this as

$$\mathbf{u}(\mathbf{r}) \approx \mathbf{u}(\mathbf{r}_0) + \Omega(\mathbf{r} - \mathbf{r}_0) + E(\mathbf{r} - \mathbf{r}_0)$$

or by expressing the antisymmetric part as a cross product

$$\mathbf{u}(\mathbf{r}) \approx \mathbf{u}(\mathbf{r}_0) + \boldsymbol{\Omega} \times (\mathbf{r} - \mathbf{r}_0) + E(\mathbf{r} - \mathbf{r}_0)$$

where $E = \frac{1}{2}(A + A^T)$ and $\Omega = \frac{1}{2}(A - A^T)$. These are referred to as the *strain* and *vorticity* of the flow. Please note that different authors can put the factor of two in different places, which can make a difference in the constitutive equation later.

A note for the careful reader, some of the equations in the following implicitly makes use of differential tensor operations using the ∇ operator. As it is not really relevant to the rest of this document, and does not add to clarity of this brief overview, we will not go into the details here. To perform the derivation of Navier-Stokes carefully, the reader is recommended to consult a textbook on fluid mechanics, such as [9].

2.1.2 Navier-Stokes

Continuum mechanics, of which fluid mechanics is a subset, builds on the continuum hypothesis. Basically matter is discrete, a fluid is built of many molecules interacting all the time. To use differential calculus as a working tool, matter needs to be continuous. The hypothesis is simply that there exists an element much larger than the mean free path of individual molecules, but still small enough to be treatable as a differential element. This turns out to work well in many cases, but not for example in rarefied, extremely low density, gases.

The equations governing fluid dynamics are expressions of conservation laws. An intuitive way to think about them is that each conserved quantity should be conserved for a fluid element, a control volume. Using Gauss and Stokes' vector theorems the laws are expressed in differential form, valid for a point. There is

- mass conservation,
- momentum conservation and
- energy conservation.

We will consider isothermal conditions, where the energy equation does not explicitly come into play. Conservation of mass is referred to as a continuity equation, in its differential form it reads

$$\frac{\partial \rho}{\partial t} + \nabla \cdot (\rho \mathbf{u}) = 0,$$

2.1. FLUID DYNAMICS

where ρ is the local density and \mathbf{u} is the flow field. The equation describes time change of density in the first term, which must equal the net material flow in the second term. It is customary to define the *material derivative*

$$\frac{D}{Dt} = \frac{\partial}{\partial t} + \mathbf{u} \cdot \nabla,$$

under which the continuity equation becomes

$$\frac{D\rho}{Dt} + \nabla \cdot \mathbf{u} = 0.$$

The interpretation of D is a vector derivative taken along a path of the flow. Momentum conservation in a fluid element leads to *Cauchy's momentum equation*

$$\rho \frac{D\mathbf{u}}{Dt} = \nabla \cdot \boldsymbol{\sigma}$$

where the new variable $\boldsymbol{\sigma}$ is the flow *stress tensor*. It relates the stress, force per area, to the deformation of a fluid element. The specification of $\boldsymbol{\sigma}$ is called a *constitutive equation*. Without further detail, the constitutive equations can be very complicated in general cases. We are, however, interested in well-behaved fluids like water. These so called *Newtonian* fluids have a linear relation between strain and stress, and the linear coefficient is the viscosity μ of the fluid. Further since we will deal with liquid phase, we say that our Newtonian fluid is also incompressible. Under these assumptions the stress tensor has the form

$$\boldsymbol{\sigma} = -p\delta + 2\mu E$$

where E is the strain of the flow field and δ is the unit tensor. Now, inserting the constitutive equation into Cauchy's momemtum equation leads to the Navier-Stokes equation for an incompressible, Newtonian fluid:

$$\rho \frac{D\mathbf{u}}{Dt} = -\nabla p + \mu \nabla^2 \mathbf{u}$$

Excluding external forces, this is the form Navier derived in 1827. The condition of incompressibility is stated differentially as

$$\nabla \cdot \mathbf{u} = 0,$$

which means that the same amount that flows into a control volume must also flow out somewhere else. The boundary conditions usually adopted when solving Navier-Stokes is the *no-slip* boundary,

$$\mathbf{u}(\mathbf{r}) = 0, \quad \mathbf{r} \in S.$$

It states that a fluid adheres to a solid interface, having zero vector velocity at boundaries. The no-slip condition is an experimental fact, and holds well as long as the molecular mean free path is small compared to the geometric dimensions of the flow.

2.1. FLUID DYNAMICS

2.1.3 From Navier to Stokes

Even the simplified case of a Newtonian and incompressible fluid turns out to be ridiculously difficult to solve, or even analyze. Conventional PDE techniques have not even found a proof of existence of solutions. One of the Millennium Problems posed by The Clay Mathematics Institute promises an award of \$1 million for a proof of existence or breakdown of these equations.¹

There are however cases admitting some analytic progress, one such is the low Reynolds number limit, or *creeping motion*. Loosely speaking this is the limit of fluids in slow motion, or at very high viscosity. This normally results in well-behaved laminar flow. If we expand the material derivative, the Navier-Stokes equation can be written as

$$\rho \left(\frac{\partial \mathbf{u}}{\partial t} + \mathbf{u} \cdot \nabla \mathbf{u} \right) = -\nabla p + \mu \nabla^2 \mathbf{u}.$$

Consider the steady state equation

$$\underbrace{\rho \mathbf{u} \cdot \nabla \mathbf{u}}_{\text{Inertial forces}} = -\nabla p + \underbrace{\mu \nabla^2 \mathbf{u}}_{\text{Viscous forces}}.$$

where inertial forces are due to the fluid mass in motion, and the viscous forces are due to internal stress from deformation of fluid elements. Say there is some characteristic flow speed U , and a characteristic length scale L . The latter typically represents the smallest dimension available, for example the width of a pipe, or the radius of a sphere around which a fluid flows. Rescaling the equations by

$$\begin{aligned} \mathbf{r}' &= \frac{\mathbf{r}}{L}, \\ \mathbf{u}' &= \frac{\mathbf{u}}{U}, \\ p' &= \frac{p}{\mu U / L} \end{aligned}$$

yields a dimensionless form

$$\frac{UL\rho}{\mu} \mathbf{u}' \cdot \nabla \mathbf{u}' = -\nabla p' + \nabla^2 \mathbf{u}'.$$

where the dimensionless group $\frac{UL\rho}{\mu}$ is called the Reynolds number. If the Reynolds number is very small, we can drop the left hand side and arrive at Stokes creeping motion equations

$$\begin{aligned} \mu \nabla^2 \mathbf{u} &= \nabla p \\ \nabla \cdot \mathbf{u} &= 0 \end{aligned} \tag{2.1}$$

For the Reynolds number to be small, we to some degree have to fulfill

¹http://www.claymath.org/millennium/Navier-Stokes_Equations/

2.2. HYDRODYNAMICS OF PARTICLES

- low flow rate,
- small dimensions,
- low density fluid or
- high viscosity.

Sometimes the quantity $\nu = \mu/\rho$ [m²/s] is called the *kinematic viscosity*, as it does not have any units of mass. As a relevant order of magnitude example, consider a microchannel with pressure driven water flow at room temperature. Say $L \approx 100 \mu\text{m}$, $U \approx 100 \mu\text{m}/\text{s}$. The kinematic viscosity of water at room temperature is about $10^{-6} \text{ m}^2/\text{s}$. The Reynolds number is

$$\text{Re} = \frac{UL}{\nu} = \frac{10^2 \cdot 10^{-6} \cdot 10^2 \cdot 10^{-6}}{10^{-6}} = 10^{-2}$$

The Reynolds number is a very common scalar classifier of flows, but care has to be taken when comparing between different situations. The inherent arbitrariness in choosing scaling dimensions limits the number to a coarse grained dynamic simility test, not an exact tool. There is also a distinction between Reynolds numbers for a flow, and Reynolds number for a particle immersed in the flow. Length scales and densities may differ, and even though inertial effects are small for the ambient flow, the particle may be heavy enough to experience inertial forces. For the remainder of this report the assumption is that all involved scales are small enough to admit a low Reynolds approximation.

2.2 Hydrodynamics of particles

We are mainly interested in what happens to a particle placed in a flow. In the previous section we discussed how flow at low Reynolds numbers appears inertialess. The same applies to sufficiently small and light particles. Newton's dynamical law reduces to the force balance

$$m\mathbf{a} = \mathbf{F} = \mathbf{0}.$$

The force can be split into two parts: hydrodynamic forces \mathbf{F}_H and external forces \mathbf{F}_E . The latter can be for example electromagnetic interaction or gravity. Right now we will focus on the hydrodynamic force arising from the fluid interaction. Since this force generally depends on the particle velocity, Newton's second order equation of motion reduces to a first order differential equation. A well-known example is that of Stokes drag on a spherical particle

$$\mathbf{F}_H = -\gamma(\mathbf{u}(\mathbf{r}_0, t) - \dot{\mathbf{r}}_0) = \mathbf{0},$$

where \mathbf{u} is the flow velocity field and \mathbf{r}_0 is a reference point on the rigid body. This force balance leads to simple advection of the particle along the flow. We will return to this at the end of this section.

2.2. HYDRODYNAMICS OF PARTICLES

Now we ask the more general question: what is the hydrodynamic force \mathbf{F}_H ? The answer any textbook on hydrodynamics will give is: the flow stress tensor σ integrated over the particle surface S ,

$$\mathbf{F}_H = \int_S \sigma \cdot d\mathbf{S} \quad (2.2)$$

Now the question is instead, what is the stress tensor σ ? For an incompressible, Newtonian fluid it is a linear function of the pressure p and the flow Jacobian $A = \nabla \mathbf{u}$

$$\sigma = -p\delta + 2\mu E, \quad E = \frac{1}{2}(A + A^T)$$

where δ is the unit tensor. For low Reynolds numbers the flow dynamics are governed by the creeping motion Stokes equations as motivated in the previous sections. They are repeated here for convenience:

$$\begin{aligned} \mu \nabla^2 \mathbf{u} &= \nabla p \\ \nabla \cdot \mathbf{u} &= 0 \\ \mathbf{u}(\mathbf{r}) &= \mathbf{0} \quad \mathbf{r} \in S \end{aligned} \quad (2.3)$$

These are to be solved with no-slip boundary conditions in a geometry as in figure

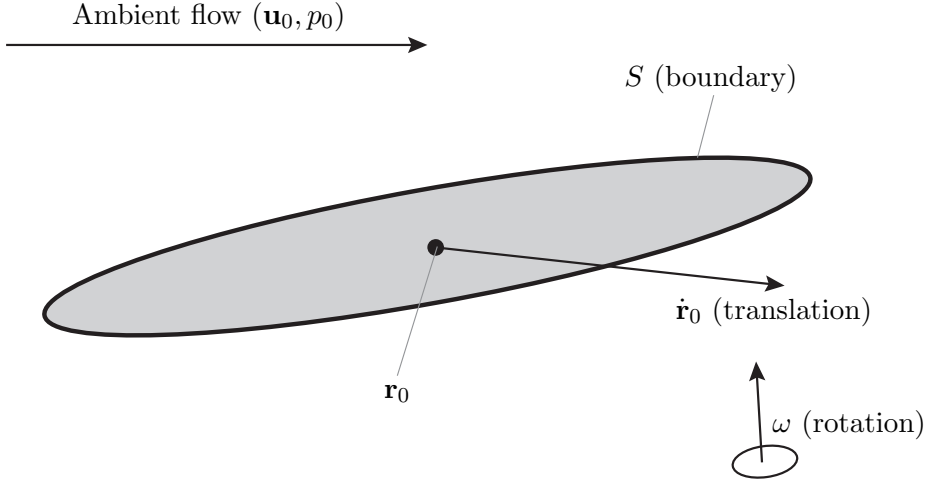


Figure 2.1: Boundary geometry to the Stokes equations. A rigid particle is immersed in an ambient flow (\mathbf{u}_0, p_0) while undergoing motion described by velocity $\dot{\mathbf{r}}_0$ and rotation ω .

2.1. We will now briefly see how the linearity of the Stokes equations are the key to computing the hydrodynamic force.

2.2. HYDRODYNAMICS OF PARTICLES

Assume there is an ambient flow (\mathbf{u}_0, p_0) , which is a solution to (2.3) in the given geometry without the particle present. On immersing a particle in the flow, the flow changes locally. Say (\mathbf{u}_D, p_D) is a disturbance due to the particle such that

$$\begin{aligned}\mathbf{u} &= \mathbf{u}_0 + \mathbf{u}_D \\ p &= p_0 + p_D\end{aligned}$$

solves (2.3). By linearity of the Stokes equations the disturbance field must also be a solution.

The particle is moving with a velocity $\dot{\mathbf{r}}_0$ and a rotation ω relative to the reference point \mathbf{r}_0 . The appropriate, dynamic, no-slip boundary condition is then

$$\mathbf{u}_0 + \mathbf{u}_D = \dot{\mathbf{r}}_0 + \omega \times (\mathbf{r} - \mathbf{r}_0), \quad \mathbf{r} \in S. \quad (2.4)$$

In addition, the disturbance (\mathbf{u}_D, p_D) should vanish as \mathbf{r} goes to infinity away from the particle. Assuming that the particle is small compared to characteristic lengths of the flow, we can linearize the ambient flow and rewrite the condition (2.4) as

$$\mathbf{u}_D = \underbrace{\dot{\mathbf{r}}_0 - \mathbf{u}_0(\mathbf{r}_0)}_{\text{Translation}} + \underbrace{(\omega - \boldsymbol{\Omega}_0) \times (\mathbf{r} - \mathbf{r}_0)}_{\text{Rotation}} - \underbrace{E_0(\mathbf{r} - \mathbf{r}_0)}_{\text{Strain}}, \quad \mathbf{r} \in S. \quad (2.5)$$

Again due to linearity the problem can be solved separately for the three different terms in the boundary condition. The translation part corresponds physically to the problem of a steadily moving particle in a quiescent fluid. The rotation corresponds to a steadily rotating particle in a quiescent fluid and the strain part is equivalent to solving a fixed particle in a linear flow. The stress contributions from all these solutions can simply be added, and the hydrodynamic force (2.2) is

$$\begin{aligned}\mathbf{F}_H &= \int_S \sigma \cdot d\mathbf{S} \\ &= \int_S (\sigma_T + \sigma_R + \sigma_S) \cdot d\mathbf{S} \\ &= \mathbf{F}_T + \mathbf{F}_R + \mathbf{F}_S\end{aligned}$$

where subscripts correspond to translation, rotation and shear, respectively.

In the 1960's Brenner and collaborators [10] showed that both hydrodynamic force and torque on particles of arbitrary shape in a linear flow are on the form

$$\begin{bmatrix} \mathbf{F}_H \\ \mathbf{T}_H \end{bmatrix} = \mu \begin{bmatrix} A & D & G \\ D^T & B & H \end{bmatrix} \begin{bmatrix} \dot{\mathbf{r}}_0 - \mathbf{u}_0(\mathbf{r}_0) \\ \omega - \boldsymbol{\Omega}_0 \\ E_0 \end{bmatrix} \quad (2.6)$$

where the so called material tensors A , B , D , G and H only depend on the particle geometry. They are obtained by solving the corresponding Stokes problems. In general this is very difficult, but numerically quite tractable [11].

2.3. RHEOLOGY OF SUSPENSIONS

For practical analysis this general formulation is cumbersome, but it tells us one very important and non-trivial thing. It can be shown [10] that for orthotropic² particles the coupling tensor D vanishes. That means translational and rotational motion can be treated separately.

For a sphere the only non-vanishing material tensors are $A = 6\pi a^1$ and $B = 8\pi a^2 \mathbf{1}$. By insertion in (2.6) and letting the hydrodynamic force to zero, we see that a sphere is advected along streamlines and rotated with the flow vorticity. Since a sphere is orthotropic, no coupling occurs between translation and rotation. For the case of ellipsoids, which we will talk about at length later, the difference is that the strain-coupling tensor H is non-zero. The ellipsoid is also advected, but its rotation is affected by a straining force which in effect tries to align the particle with the flow. The basic solution for this case is discussed in section 2.4 and our analysis follows in chapter 3.

2.3 Rheology of suspensions

From the Greek word *rheo* meaning flow, rheology is the study of flows. More specifically it is the study of interesting material flows [12]. It is inherently interdisciplinary as it aims to understand diverse phenomenon from magma currents in geology, structural integrity of concrete to the texture of food. A rheological question anyone can have is: It takes a lot of force to stir honey, even though it flows if left alone. Mayonnaise is very easily stirred, but it stays in the shape you leave it. What is the difference?

Although the main topic of this thesis is not rheology, it deals with it implicitly. The pioneering work in the field of particle dynamics in flows started out to explain how the viscosity of a medium changes due to suspended particles. Rheology is much more than just viscosity, and the interested reader is encouraged to read Wikipedia's article on rheology at <http://en.wikipedia.org/wiki/Rheology>.

2.3.1 Viscosity

The viscosity of a fluid is essentially its resistance to flow. More specifically it is the resistance to deformation of a fluid element. The solid analog is Hooke's law which relates the displacement x to the reactive force F via a constant of elasticity k as

$$F = -kx.$$

Newton's viscosity law relates a *rate of displacement* $\frac{dx}{dy}$ to the reactive stress τ , via a constant of viscosity μ as

$$\tau = \mu \frac{dx}{dy}.$$

The stress τ can be thought of as the drag, if you will, and the rate of displacement is the corresponding velocity. Just as not all solid materials display perfect linear behaviour in

²An object with three orthogonal symmetry planes

2.4. ELLIPSOID DYNAMICS

elasticity, do not all fluids display linear viscosity. Fluids which in experiment do follow Newton's law of viscosity are called *Newtonian*. The prime example is regular water. Non-newtonian fluids come in many varieties, differing from the Newtonian viscosity relation in different ways. An example which might be familiar is ketchup which is initially very viscous, but loosens up under shear. More shear leads to smaller resistance over time.

Viscosity is due to internal mechanical dissipation. One form we are particularly interested in is the one induced by particle motion in the flow. For incompressible, Newtonian fluids it is a matter of integrating a function of the flow strain tensor over the fluid volume [10].

2.3.2 Einstein's 1906 result

As in many other fields, Einstein provided one of the founding papers for particle motion in fluids [1]. In his doctoral dissertation *Eine neue bestimmung der moleküldimensionen* he devised a method of measuring the size of molecules indirectly by measuring viscosity. As a means to this end he solved the Stokes equations for a rigid sphere in a linear flow. He found that the particle is advected, and that it rotates around the flow vorticity axis. Einstein calculated the increase in energy dissipation due to the particle. Assuming that the suspension is dilute so that particle interactions can be neglected, this lead to the effective viscosity

$$\hat{\eta} = \eta \left(1 + \frac{5}{2}\phi\right)$$

where ϕ is the volume fraction of particles in the liquid.

2.4 Ellipsoid dynamics

As an extension of Einstein's work, Jeffery considered suspensions of ellipsoidal particles [3]. That is particles which can be geometrically described by

$$\left(\frac{x}{a}\right)^2 + \left(\frac{y}{b}\right)^2 + \left(\frac{z}{c}\right)^2 = 1.$$

Jeffery solved the resulting force and torques on an ellipsoidal particle in a linear flow. Oberbeck [13] already 1876 showed that the ellipsoid is advected. Jeffery used this and computed a resulting torque with two terms acting on the moving ellipsoid. One term rotates the particle around the flow vorticity axis. The second term attracts the particle to align with the flow direction. In general these two terms give rise to very complicated dynamics [14].

In particular, Jeffery integrated the equation of motion for a simple shear flow, and an axisymmetric particle. A shear flow in the $\hat{\mathbf{z}}$ -direction is described by

$$\mathbf{u} = \alpha x \hat{\mathbf{z}}$$

2.4. ELLIPSOID DYNAMICS

where $\hat{\mathbf{x}}$ is the shearing direction, in which shear strength increases. $\hat{\mathbf{y}}$ is the vorticity direction, around which particles rotate. A drawing of this coordinate system is shown in figure 2.2.

An axisymmetric ellipsoid is such that two of its half-axes are equal. They are also referred to as spheroids and can be described by

$$\frac{x^2 + y^2}{a^2} + \frac{z^2}{b^2} = 1.$$

The unique axis, in this case z , is called the principal axis. The important property of the spheroid is its aspect ratio $\lambda = \frac{b}{a}$. In 1962, Bretherton [15] showed that Jeffery's results are valid for almost any axisymmetric particle using an effective aspect ratio. By

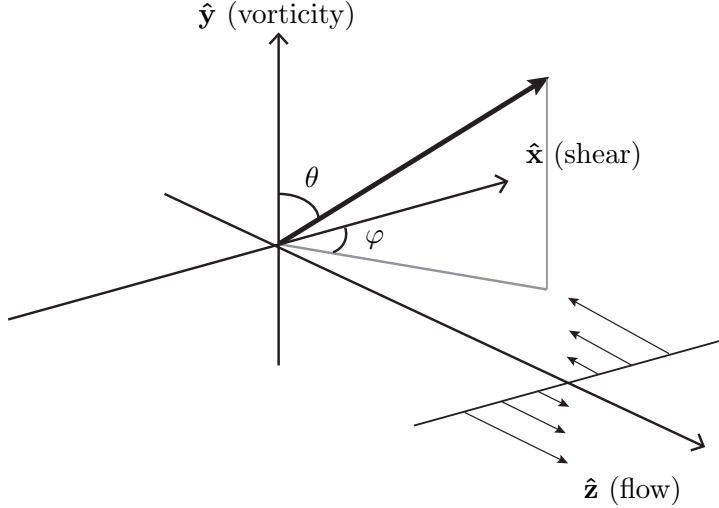


Figure 2.2: Coordinate system used in describing Jeffery's results. $\hat{\mathbf{z}}$ is the flow direction. $\hat{\mathbf{x}}$ is the shearing direction, in which shear strength increases. $\hat{\mathbf{y}}$ is the vorticity direction, around which particles rotate. A spherical coordinate system (θ, φ) is used to describe the Jeffery orbits.

integrating the equation of motion Jeffery found that the ellipsoids rotate in one of a family of one-parameter closed orbits. Which one is entirely decided by initial conditions. More specifically, attach a unit vector $\hat{\mathbf{n}}$ to the principal axis of the ellipsoid. Describe it in spherical coordinates as specified in figure 2.2. Then the motion is described by

$$\tan \varphi = \frac{1}{\lambda} \tan \omega t \quad (2.7)$$

$$\tan \theta = C \sqrt{\lambda^2 \cos^2 \omega t + \sin^2 \omega t} \quad (2.8)$$

$$\omega = \frac{\alpha \lambda}{\lambda^2 + 1}$$

which are closed orbits with period time

$$T = \frac{2\pi}{\omega} = 2\pi \frac{\lambda^2 + 1}{\alpha\lambda}$$

The undetermined C is the *orbit constant*, decided by initial condition. These equations describe the so called Jeffery orbits.

There were no direct observations of single particles in 1922, and Jeffery's main result was an extension of Einstein's 1906 viscosity calculation. Particles aligned along the flow dissipate less energy than particles orthogonal to the flow. He showed that the result is still on the Einstein form

$$\hat{\eta} = \eta(1 + \nu\phi)$$

But since there is an indeterminacy in the orbit constant C Jeffery could but provide an upper and a lower bound for ν . This, however, is not the main interest of this report. We are interested in the motion of individual particles. In the following sections we will take a closer look at the Jeffery orbits and the indetermined constant.

2.4.1 The Jeffery orbits

The Jeffery orbits are one-parameter closed orbits, with the one parameter being time. That means as time goes on, the particle orientation returns to the initial condition. Again, visualize a unit vector $\hat{\mathbf{n}}$ to the principal axis of the ellipsoid, then the tip of the vector traces orbits like in figure 2.3. The orbits are symmetric around the flow vorticity axis, indicated in the figure. Different aspect ratios deform the orbits. For a particle of aspect ratio 1, a sphere, the orbits are perfectly circular whereas higher aspect ratio deforms the orbits.

As indicated by the orbit equations (2.7) the orbit constant $C = 0$ corresponds to the degenerate orbit which is only a point at the vorticity direction. The other limit as $C \rightarrow \infty$ corresponds to the circular orbit in the flow-shear plane. In chapter 3 we will see how this constant relates geometrically to the tangens of an angle.

2.4.2 Particle orientation distribution

To calculate rheological properties it is necessary to perform ensemble averages over many particles. Therefore many authors have investigated the orientation distribution of the ellipsoids. If a particle follows a specific orbit C there is a conditional joint distribution

$$P(\theta, \varphi, t | C)$$

The hard question is: what is the distribution of the orbit constant? Given that, it is a trivial matter of multiplication to find the orientation distribution

$$P(\theta, \varphi, t) = P(\theta, \varphi, t | C)P(C, t)$$

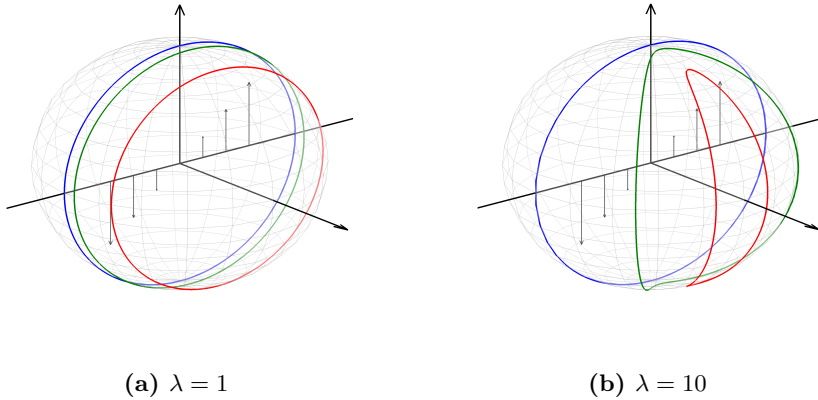


Figure 2.3: Sample of Jeffery orbits. North pole indicates the flow direction, with shear flow as annotated by arrows. Imagine a unit vector $\hat{\mathbf{n}}$ in origo, attached to the principal axis of the ellipsoid. As time propagates the tip of $\hat{\mathbf{n}}$ traces the shown orbits. Different orbits correspond to different orbit constants C . The left image is generated using aspect ratio 1, a sphere, the right with aspect ratio 10, an ellipsoid.

Eisenschitz [16] postulated that the particles would be uniformly distributed on the sphere. Extensive work on explaining the orbit distribution with isotropic Brownian noise has been done by Hinch & Leal [17][18]. Rahnama et al [19] considered the extension to anisotropic Brownian noise to explain particle-particle interactions in experimental data. Although interesting in its own right, we will not digress further here as our current work is concerned with one particular orbit, not the results of an average.

2.4.3 Infinite aspect ratio models

Inspired by single polymer experimental observations Turitsyn et al [20] developed an alternative theory for rods of infinite aspect ratio. According to Jeffery's calculations a particle of infinite aspect ratio aligns with the flow field and stays there. Turitsyn's hypothesis is that the dynamics are noise-driven. In presence of some noise the metastable aligned state is aperiodically perturbed to initiate a flip. As soon as the flow gets hold of the particle the flip is driven by hydrodynamics until almost aligned at the opposite direction. A schematic illustration of this is found in figure 2.4. Using this combination of stochastic and deterministic dynamics Turitsyn calculates characteristics of angle distributions as well as a prediction on the distribution of time between flips.

2.4. ELLIPSOID DYNAMICS

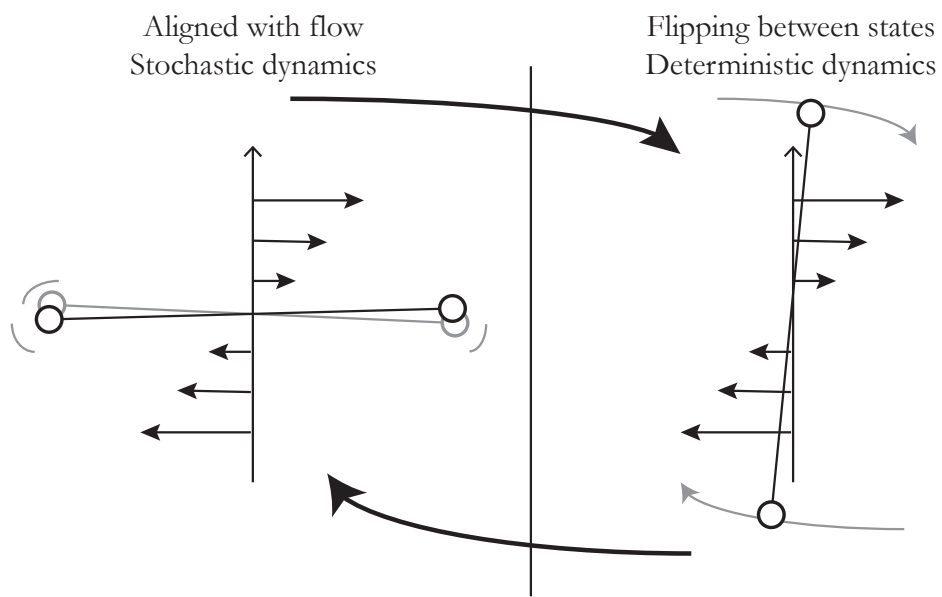


Figure 2.4: Schematic illustration of Turitsyn's infinite aspect ratio dumbbell model. The meta-stable aligned state is perturbed to initiate a flip (Stochastic dynamics, to the left). As soon as the flow gets hold of the particle the flip is driven by hydrodynamics until almost aligned at the opposite direction (Deterministic dynamics, to the right.)

3

Dynamics of rods in viscous flows

EVERYTHING STARTED WITH a movie from a neighbouring experimental group. A polymer rod, about $20\text{ }\mu\text{m}$ in length, racing through a microchannel. It is aligned with the flow but flips 180 degrees between the two degenerate states, with almost constant period as predicted by Jeffery. Our investigation starts with the well-known Jeffery orbits, an amazingly close fit. Where the theory predicts closed orbits, we observe drift or jumps between different. This chapter describes our efforts in understanding the motion of the rods in the microchannel.

First the experimental data will be described. The theory part will start through an alternative derivation of the Jeffery equations including a slight generalization. We will show this to reduce to Hinch & Leal's reformulation from the 1970's. Then we will develop a geometric intuition for the Jeffery equation and see how the original orbit equations arise in a natural way. A qualitative comparison of theory and experimental observations will be presented before the chapter is concluded with an overview of present work and where we are heading right now, experimentally and theoretically.

3.1 Experimental data

The experiments are performed in a microchannel. A constant pressure driven flow advects rigid rodlike particles along the channel. The rod is observed from a top view using a video camera on a microscope. An operator manually tracks the particles along the channel using a joystick. Complete details of the experiment is available in Oladiran's Master's thesis [2].

3.1.1 Movies

For all data presented here a channel of cross section $400\text{ }\mu\text{m}$ wide and $100\text{ }\mu\text{m}$ high has been used. The raw data available is movies at 10 Hz and 979×515 pixels in resolution.

3.1. EXPERIMENTAL DATA

A sample screenshot is shown in figure 3.1. The raw data shows one particle along the channel. Typically the time series is 60–120 s long at 10 Hz.

Qualitatively, the particles appears to align with the flow direction most of the time. What is interesting is that they flip 180 degrees periodically, as predicted by Jeffery. But we also observe a paddling behavior where the particle never really aligns with the flow direction. There exists Jeffery orbits which have this characteristic.

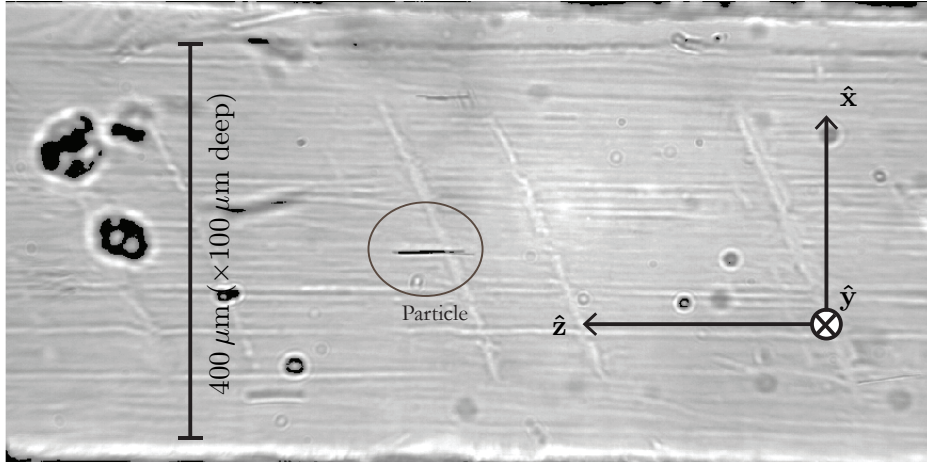


Figure 3.1: Experimental data sample screenshot. The raw image is 979×515 pixels in resolution and show a microchannel seen from the top. The channel is $400 \mu\text{m}$ wide and $100 \mu\text{m}$ high. The coordinate system is moving along with the advected particle.

3.1.2 Analysis

We are interested in the orientation of particles as time series. Since we are observing from a single direction, we have only a 2-dimensional projection of the 3-dimensional dynamics. Therefore we estimate the length of the particle which determines the 3-dimensional dynamics up to sign on the depth axis. The coordinate system used and a schematic of the projection is shown in figure 3.2. A Matlab program was written which plays the movie one frame at a time and takes as input two mouse clicks specifying the endpoints of the rod at each frame. These were cropped in time to remove boundary effects from inlet and outlet of the microchannel. This projected data can be transformed to a direction on the unit sphere and visualized as in figure 3.3. The north pole corresponds to the positive flow direction. The path is noisy due to the measurements. It is practically impossible to see a difference between different paths near the flow direction, corresponding to north and south poles. Note how the path taken is similar to the Jeffery orbits. A complementary visualization is used, where the vector is projected on the three cartesian axes as a function of time. This shows the periodic tumbling behavior with long periods aligned with the flow, interrupted by sudden flips. We will return to this data, but first we will develop our theoretical view of the particle dynamics.

3.1. EXPERIMENTAL DATA

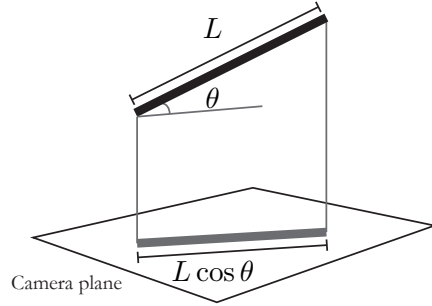


Figure 3.2: With knowledge of the particle length L , the projection on the camera plane allows computation of the orientation up to a sign in the depth axis.

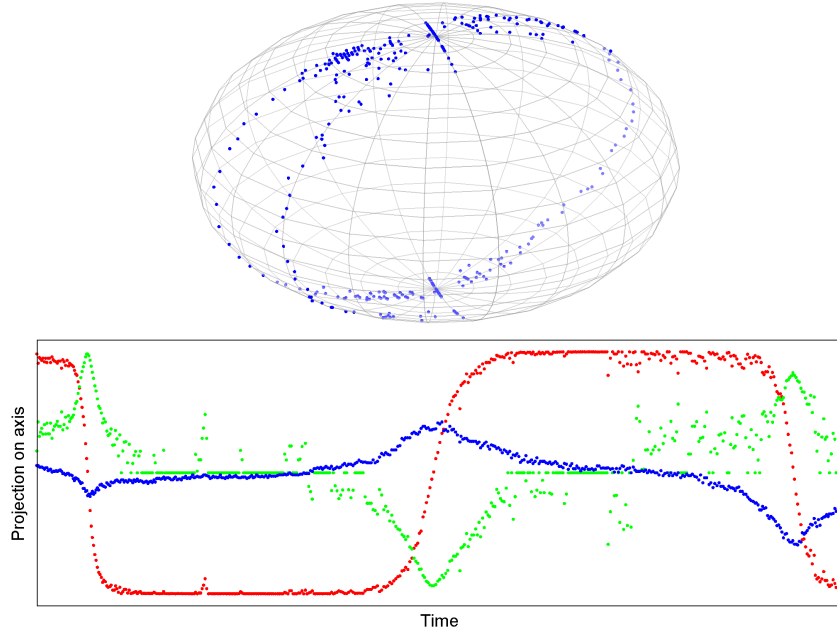


Figure 3.3: Data from the first experimental observation. Points on sphere (top) represent orientation of an axisymmetric particle. The north pole corresponds to aligned with the positive flow direction. Imagine the rod particle attached to origo, and its principal axis pointing in direction of a point. Bottom shows the time series of the principal axis projected on the three cartesian axis. Noise between flips is from difficulties separating directions close to flow alignment.

3.2 Dumbbell model

A dumbbell model consists of small rigid spheres, *beads*, which are connected. Many variations of dumbbell models are used in modeling of polymers. We recommend volume 2 of Bird's book [21] for a good overview. We are using the simplest possible variant where beads are connected by rigid rods, essentially creating a rigid body of point masses. Each bead is affected by the Stokes force,

$$\mathbf{F}_i = \gamma_i(\mathbf{u}(\mathbf{r}_i) - \dot{\mathbf{r}}_i), \quad (3.1)$$

and hydrodynamic interaction between beads are ignored.

An ellipsoid particle is modeled as three dumbbells crossed perpendicularly. The three dumbbells have lengths $2a_i$ where a_i corresponds to the half-axes of the ellipsoid modeled. The 3-dimensional dumbbell is depicted in figure 3.4a. We have a rigid body and therefore 6 degrees of freedom. The equations of motion in the low Reynolds number regime are force and torque balance.

According to the more general hydrodynamic theory in chapter 2, a particle of this type would be advected at its center of mass. It is easily shown that is the case for *linear flows* as follows. The total force on the dumbbell is

$$\begin{aligned} \mathbf{F} &= \sum_i \gamma_i(\mathbf{u}(\mathbf{r}_i) - \dot{\mathbf{r}}_i) \\ &= \sum_i \gamma_i \mathbf{u}(\mathbf{r}_i) - \sum_i \gamma_i \dot{\mathbf{r}}_i \end{aligned}$$

define the *total friction* $\Gamma = \sum_i \gamma_i$ and the *center of friction* $\mathbf{r}_\gamma = \Gamma^{-1} \sum_i \gamma_i \mathbf{r}_i$ and linearize the flow with jacobian A to get

$$\begin{aligned} &= \sum_i \gamma_i (\mathbf{u}(\mathbf{r}_\gamma) + A(\mathbf{r}_i - \mathbf{r}_\gamma)) - \Gamma \dot{\mathbf{r}}_\gamma \\ &= \Gamma \mathbf{u}(\mathbf{r}_\gamma) - \Gamma \dot{\mathbf{r}}_\gamma + \sum_i A(\mathbf{r}_i - \mathbf{r}_\gamma) \end{aligned}$$

but for any particle which has the beads symmetrically distributed around \mathbf{r}_γ , our dumbbell in particular, the last sum vanishes identically and we arrive at the result

$$= \Gamma(\mathbf{u}(\mathbf{r}_\gamma) - \dot{\mathbf{r}}_\gamma)$$

We are now interested in deriving the equation of motion for the orientation of the dumbbell.

3.2.1 Rotation matrix equation of motion

Consider representing the orientation as a rotation matrix R . Define the dumbbell on a cartesian set of axes $\{\mathbf{e}_i\}_{i=x,y,z}$. Particle center on origo and half-axes extending along

3.2. DUMBBELL MODEL

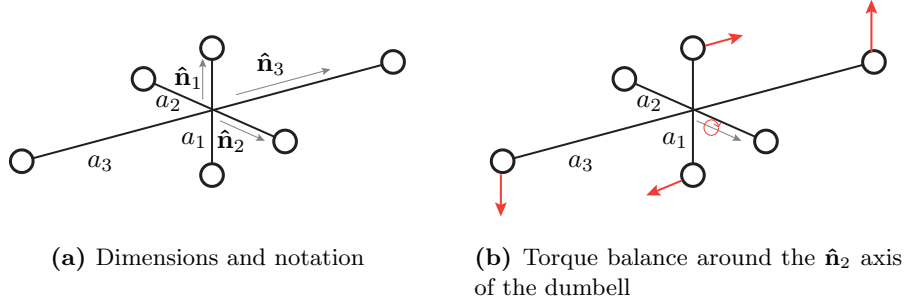


Figure 3.4: 3-dimensional dumbbell model representing ellipsoidal particles. The axes $\hat{\mathbf{n}}_i$ rotate with the particle. The half axes lengths are denoted a_i .

coordinate axes with lengths a_x , a_y and a_z . Further define local particle axes which are rotating along with the particle:

$$\mathbf{n}_i(\mathbf{t}) = R(t)\mathbf{e}_i, \quad i = 1, 2, 3 \quad (3.2)$$

We want to solve for $R(t)$, and the key is to exploit the orthogonal nature of rotation matrices:

$$R^T R = 1$$

which under differentiation with respect to time gives

$$\begin{aligned} R^T \dot{R} &= -\dot{R}^T R \\ R^T \dot{R} &= -(R^T \dot{R})^T \end{aligned}$$

Define $Q = R^T \dot{R}$ and note that it is skew-symmetric and especially that $\dot{R} = RQ$. It has the form

$$Q = \begin{bmatrix} 0 & Q_{12} & Q_{13} \\ -Q_{12} & 0 & Q_{23} \\ -Q_{13} & -Q_{23} & 0 \end{bmatrix}$$

By torque balance around the three particle axes \mathbf{n}_i we get equations for the three unknowns in Q . Consider for example torque around axis \mathbf{n}_1 , see figure 3.4b.

$$0 = a_3 \mathbf{n}_2^T (\mathbf{u}_3 - 2a_3 \dot{\mathbf{n}}_3) - a_2 \mathbf{n}_3^T (\mathbf{u}_2 - 2a_2 \dot{\mathbf{n}}_2)$$

where \mathbf{u}_i is shorthand for

$$\mathbf{u}_i = \mathbf{u}(\mathbf{r}_\gamma + a_i \mathbf{n}_i) - \mathbf{u}(\mathbf{r}_\gamma - a_i \mathbf{n}_i).$$

Substitute the rotated coordinates (3.2) to get

$$0 = a_3 \mathbf{e}_2^T R^T (\mathbf{u}_3 - 2a_3 \dot{R} \mathbf{e}_3) - a_2 \mathbf{e}_3^T R^T (\mathbf{u}_2 - 2a_2 \dot{R} \mathbf{e}_2),$$

3.2. DUMBBELL MODEL

which can be rearranged to

$$\begin{aligned} -2a_3^2 \underbrace{\mathbf{e}_2^T R^T \dot{R} \mathbf{e}_3}_{Q_{23}} + 2a_2^2 \underbrace{\mathbf{e}_3^T R^T \dot{R} \mathbf{e}_2}_{-Q_{23}} &= -a_3 \mathbf{e}_2^T R^T \mathbf{u}_3 + a_2 \mathbf{e}_3^T R^T \mathbf{u}_2 \\ 2(a_3^2 + a_2^2) Q_{23} &= a_3 \mathbf{e}_2^T R^T \mathbf{u}_3 - a_2 \mathbf{e}_3^T R^T \mathbf{u}_2. \end{aligned}$$

Repeating this procedure for all three axes gives

$$Q_{ij} = \frac{a_j \mathbf{e}_i^T R^T \mathbf{u}_j - a_i \mathbf{e}_j^T R^T \mathbf{u}_i}{2(a_i^2 + a_j^2)} \quad (3.3)$$

Now $\dot{R} = RQ$ can be integrated numerically for any particle aspect ratio and flow. Integrating rotation matrices is a non-trivial task in itself. One method used is discussed in appendix A.1.

3.2.2 Finding the Jeffery equations

Linearizing the flow \mathbf{u} around \mathbf{r}_γ makes

$$\mathbf{u}_i = 2a_i A R \mathbf{e}_i \quad A = \frac{d\mathbf{u}}{d\mathbf{r}}$$

and

$$Q_{ij} = \frac{\mathbf{e}_i^T (a_j^2 R^T A R - a_i^2 R^T A^T R) \mathbf{e}_j}{a_i^2 + a_j^2} \quad (3.4)$$

We will now show how this reduces to the Jeffery equation of motion when considering the principal axis of an axisymmetric particle. We can write the matrix Q as a sum of its constituents

$$\begin{aligned} Q &= Q_{12}(\mathbf{e}_1 \mathbf{e}_2^T - \mathbf{e}_2 \mathbf{e}_1^T) + \\ &\quad + Q_{13}(\mathbf{e}_1 \mathbf{e}_3^T - \mathbf{e}_3 \mathbf{e}_1^T) + \\ &\quad + Q_{23}(\mathbf{e}_2 \mathbf{e}_3^T - \mathbf{e}_3 \mathbf{e}_2^T) \end{aligned}$$

Take $a_2 = a_1$ so the principal axis is \mathbf{n}_3 . We compute its time derivative

$$\begin{aligned} \dot{\mathbf{n}}_3 &= \dot{R} \mathbf{e}_3 \\ &= R Q \mathbf{e}_3 \\ &= Q_{13} R \mathbf{e}_1 + Q_{23} R \mathbf{e}_2 \end{aligned}$$

3.3. DYNAMICS OF AXISYMMETRIC PARTICLES

Introduce the fundamental matrix

$$B = \frac{a_3^2}{a_1^2 + a_3^2} A - \frac{a_1^2}{a_1^2 + a_3^2} A^T$$

and upon expressing the components of Q we find

$$\begin{aligned} &= (\mathbf{e}_1^T R^T B R \mathbf{e}_3) R \mathbf{e}_1 + (\mathbf{e}_2^T R^T B R \mathbf{e}_3) R \mathbf{e}_2 \\ &= (\mathbf{n}_1^T B \mathbf{n}_3) \mathbf{n}_1 + (\mathbf{n}_2^T B \mathbf{n}_3) \mathbf{n}_2 \\ &= B \mathbf{n}_3 - (\mathbf{n}_3^T B \mathbf{n}_3) \mathbf{n}_3 \end{aligned}$$

which is identical to the formulation of Jeffery's equations done by Hinch & Leal [14]. It is remarkable considering the simplicity of this model in comparison to the hydrodynamic calculations that lead Jeffery to his result. It can also be shown that the components in Q , equation (3.4), reduce exactly to Jeffery's equation of motion for a general ellipsoid in a linear flow. Hinch & Leal expressed the equation using the flow strain E and vorticity Ω as

$$\begin{aligned} \dot{\mathbf{n}} &= \Omega \times \mathbf{n} + D \mathbf{n} \times E \mathbf{n} \\ D &= \frac{a_3^2 - a_1^2}{a_3^2 + a_1^2} = \frac{\lambda^2 - 1}{\lambda^2 + 1} \end{aligned}$$

which is perfectly equivalent to our result with B expressed in D :

$$\dot{\mathbf{n}} = B \mathbf{n} - (\mathbf{n}^T B \mathbf{n}) \mathbf{n} \quad (3.5)$$

$$B = \frac{D+1}{2} A + \frac{D-1}{2} A^T \quad (3.6)$$

3.3 Dynamics of axisymmetric particles

The key insight to the following analysis is as follows. The non-linear equation of motion (3.5) describes orientational change by a linear map B , the second term describes only a renormalization to unity. Specifically it makes sure that the time derivative of \mathbf{n} is perpendicular to \mathbf{n} itself at all times. It is *equivalent* to describe the particle orientation by a vector \mathbf{q} evolving under the linear equation

$$\dot{\mathbf{q}} = B \mathbf{q} \quad (3.7)$$

and at any time recover \mathbf{n} by normalization

$$\mathbf{n}(t) = \frac{\mathbf{q}(t)}{|\mathbf{q}(t)|}.$$

According to Wilkinsson et al [5], the general proof for this equivalence was first given by Szeri in 1993 [22]. This insight has to our knowledge not been exploited to analyze

3.3. DYNAMICS OF AXISYMMETRIC PARTICLES

the Jeffery orbits. For a general flow the fundamental matrix B is a function of both time and space. Formally we say that the solution for \mathbf{q} is

$$\mathbf{q}(t) = \Phi(t)\mathbf{q}(0)$$

where $\mathbf{q}(0)$ is the initial value at $t = t_0$ and the time propagator Φ satisfies the equation

$$\dot{\Phi} = B(t)\Phi.$$

We will investigate the case of constant B , corresponding to linear and time-independent flow. Then the equation for the time propagator Φ yields a matrix exponential and the solution for \mathbf{q} is

$$\mathbf{q}(t) = e^{Bt}\mathbf{q}(0) \quad (3.8)$$

The matrix exponential is conveniently analyzed with the eigensystem of B . Recall that we are dealing with incompressible fluids where

$$\nabla \cdot \mathbf{u} = 0.$$

It follows that the flow jacobian is traceless, $\text{tr}A = 0$, and by definition so is the matrix B . This is reflected in the eigenvalues whose sum must vanish:

$$\text{tr}B = \sum_i b_i = 0$$

where b_i is the eigenvalues of B . There are two main possibilities:

- Three real, distinct eigenvalues (b_1, b_2, b_3)
 - \mathbf{q} will align with the eigenvector corresponding to the largest, dominant, eigenvalue
- One real, two complex conjugate eigenvalues $(b_1, -b_1 + i\omega, -b_1 - i\omega)$, where either
 - $b_1 > 0$, \mathbf{q} will align with the eigenvector corresponding to the real eigenvalue, or
 - $b_1 \leq 0$, \mathbf{q} will rotate, and if $b_1 < 0$ spiral outwards, in the plane spanned by the real and imaginary parts of the conjugate eigenvectors.

A traceless 3 by 3 matrix has a cubic characteristic equation which can be expressed in terms of higher power traces¹

$$-b^3 + \frac{\text{tr}B^2}{2}b + \frac{\text{tr}B^3}{3} = 0.$$

¹For a traceless matrix $\det B = \text{tr}B^3/3$

3.3. DYNAMICS OF AXISYMMETRIC PARTICLES

The two cases outlined above are identified by the discriminant Δ of the equation:

$$\Delta = \frac{1}{2}\text{tr}^3 B^2 - 3\text{tr}^2 B^3 \quad \begin{cases} > 0, \text{ Three, real, distinct roots} \\ < 0, \text{ One real and two complex conjugate roots} \end{cases}$$

The two subcases with imaginary eigenvalues can be identified by the sign of $\text{tr}B^3$. It follows that the coarse characterization of the dynamics are determined by the square and cube trace. A map of this space is shown in figure 3.5.

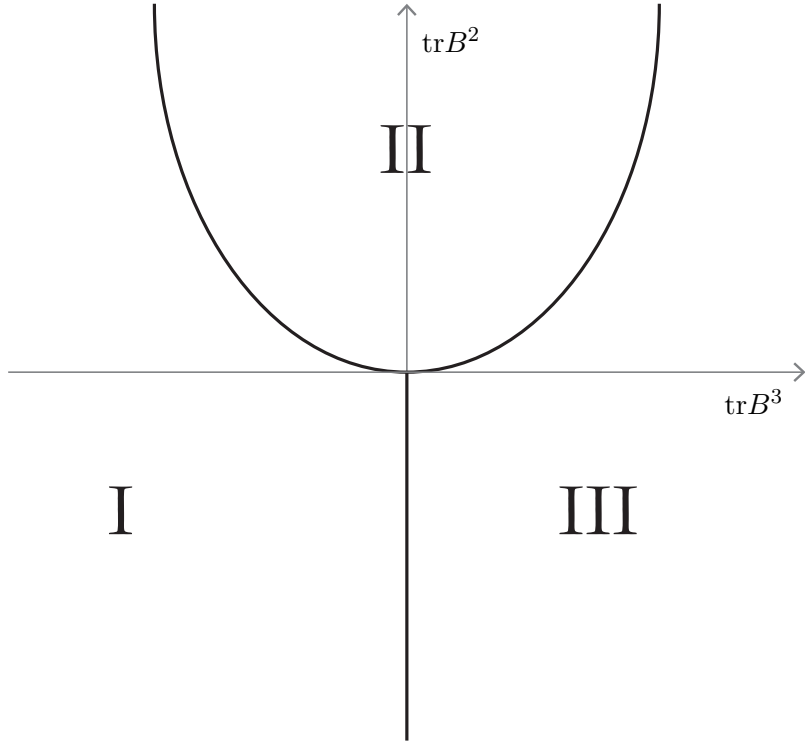


Figure 3.5: Coarse classification of the particle dynamics as a function of $\text{tr}B^2$ and $\text{tr}B^3$. In region I and II there is a dominant real eigenvalue, and we expect the particle to align with the corresponding dominant eigenvector. In region III the complex conjugate eigenvalue is dominating and we expect rotating dynamics.

To eventually relate to our experimental data we will now consider the special case of a shear flow. In the map, the shear flow is located in the lower half plane, on the $\text{tr}B^3 = 0$ line. Locally the experimental channel flow can be approximated by a flow of this kind. The idea is to find a coordinate change such that the dynamics of $\mathbf{q}(t)$ become as simple as possible. Remember that \mathbf{q} is just defined as any vector in the same direction as \mathbf{n} . This is not a well-defined one-to-one coordinate change in itself.

3.3.1 Shear flow

Consider a shear flow in the $\hat{\mathbf{z}}$ -direction, the velocity field is given by

$$\mathbf{u} = (\alpha x + \beta y) \hat{\mathbf{z}}$$

and consequently the flow jacobian is

$$A = \begin{bmatrix} 0 & 0 & 0 \\ 0 & 0 & 0 \\ \alpha & \beta & 0 \end{bmatrix}$$

Recalling the definition of B from (3.6):

$$B = \frac{1}{1 + \lambda^2} \begin{bmatrix} 0 & 0 & -\alpha \\ 0 & 0 & -\beta \\ \alpha\lambda^2 & \beta\lambda^2 & 0 \end{bmatrix}$$

where λ is the particle aspect ratio. Having $\lambda > 1$ is a cigar shaped, or *prolate*, spheroid whereas $\lambda < 1$ is a disc like, or *oblate*, spheroid. This type of matrix has three distinct eigenvalues and may be diagonalized by a matrix P as

$$B = PDP^{-1}.$$

Its eigenvalues are 0 and an imaginary conjugated pair $\pm i\omega$. As B is not a symmetric matrix, we deal with both left and right eigenvectors. The zero eigenvector \mathbf{b}_0 is the same for both left and right eigensystem. The other two are necessarily complex conjugated, like their eigenvalues. We call the right (left) vectors \mathbf{b}_R (\mathbf{b}_L) and $\bar{\mathbf{b}}_R$ ($\bar{\mathbf{b}}_L$). Expand the matrix exponential in (3.8) as follows:

$$\begin{aligned} \mathbf{q}(t) &= e^{Bt} \mathbf{q}(0) \\ &= Pe^{Dt}P^{-1}\mathbf{q}(0) \\ &= \mathbf{b}_0(\mathbf{b}_0 \cdot \mathbf{q}(0)) + e^{i\omega t} \mathbf{b}_R(\mathbf{b}_L \cdot \mathbf{q}(0)) + e^{-i\omega t} \bar{\mathbf{b}}_R(\bar{\mathbf{b}}_L \cdot \mathbf{q}(0)) \\ &= \mathbf{b}_0(\mathbf{b}_0 \cdot \mathbf{q}(0)) + 2 \operatorname{Re} \{e^{i\omega t} \mathbf{b}_R(\mathbf{b}_L \cdot \mathbf{q}(0))\} \end{aligned} \quad (3.9)$$

Now, we have a freedom in choosing $\mathbf{q}(0)$. Specifically we can choose so that $\mathbf{b}_L \cdot \mathbf{q}(0)$ is real. For notational convenience define

$$\begin{aligned} q_0 &= \mathbf{b}_0 \cdot \mathbf{q}(0) \\ q_L &= \mathbf{b}_L \cdot \mathbf{q}(0) \end{aligned}$$

and see that equation (3.9) becomes

$$\mathbf{q}(t) = q_0 \mathbf{b}_0 + 2q_L \cos \omega t \operatorname{Re} \{\mathbf{b}_R\} - 2q_L \sin \omega t \operatorname{Im} \{\mathbf{b}_R\} \quad (3.10)$$

3.3. DYNAMICS OF AXISYMMETRIC PARTICLES

Note that all choices $\mathbf{q}(0) = q_0 \mathbf{b}_0 + 2q_L \operatorname{Re}\{\mathbf{b}_R\}$ are valid, this is an entire plane through origo. Already from (3.10) we can see that the dynamics are constant in one direction, and a periodic oscillation in a plane spanned by the real and imaginary parts of \mathbf{b}_R . The oscillation is periodic with time $T = 2\pi/\omega$ which coincides with the Jeffery period time. We will return to this shortly, first some care has to be taken of this new basis.

The vector triplet $(\mathbf{b}_0, \operatorname{Re}\{\mathbf{b}_R\}, \operatorname{Im}\{\mathbf{b}_R\})$ is pairwise orthogonal. But the last two are not unit vectors. Moreover we would like to constraint the choice of $\mathbf{q}(0)$ to a curve instead of an entire plane, to remove the redundancy. It turns out that constraining $\mathbf{q}(0)$ to the upper half unit sphere makes for a good choice, as equation (3.10) becomes

$$\mathbf{q}(t) = q_0 \mathbf{b}_0 + \sqrt{1 - q_0^2} \cos \omega t \mathbf{b}_{Re} - \frac{|\operatorname{Im}\{\mathbf{b}_R\}|}{|\operatorname{Re}\{\mathbf{b}_R\}|} \sqrt{1 - q_0^2} \sin \omega t \mathbf{b}_{Im}$$

where \mathbf{b}_{Re} and \mathbf{b}_{Im} are the normalized directions. Further the ratio between the imaginary and real part vector is just $\frac{1}{\lambda}$. Identify q_0 and $-\omega t$ with angles by

$$\begin{aligned} q_0 &= \cos \gamma \\ -\omega t &= \eta. \end{aligned}$$

The result is that $\mathbf{q}(t)$ lives on an ellipsoid with aspect ratio λ :

$$\mathbf{q}(t) = \cos \gamma \mathbf{b}_0 + \sin \gamma \cos \eta \mathbf{b}_{Re} + \frac{1}{\lambda} \sin \gamma \sin \eta \mathbf{b}_{Im}$$

Which is an ellipsoid described by

$$x^2 + (\lambda y)^2 + z^2 = 1$$

where we are associating the $\hat{\mathbf{x}}$ -direction with \mathbf{b}_{Re} , $\hat{\mathbf{y}}$ with \mathbf{b}_{Im} and $\hat{\mathbf{z}}$ with \mathbf{b}_0 . In these coordinates the time dynamics are very simple:

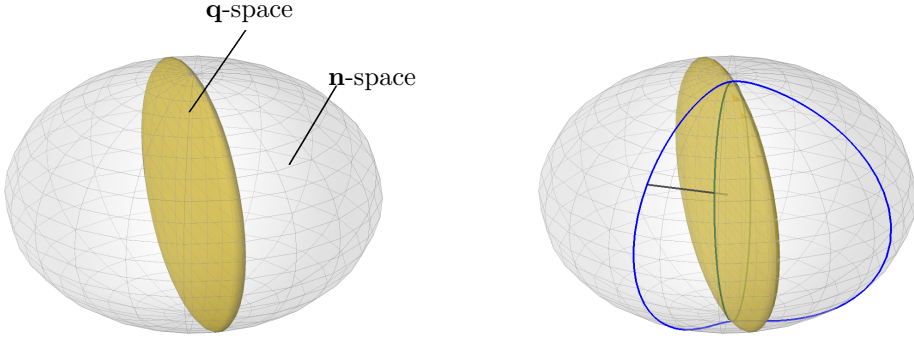
$$\begin{aligned} \dot{\gamma} &= 0 \\ \dot{\eta} &= -\omega \end{aligned}$$

Which means that $\mathbf{q}(t)$ describes closed ellipses in a fixed plane.

3.3.2 Projection into Jeffery orbits

Although we found a nice representation (γ, η) for the particle dynamics in a shear flow, the observable reality is represented by \mathbf{n} which lives on the unit sphere. Each point (q_x, q_y, q_z) on the ellipsoid corresponds to one point (n_x, n_y, n_z) on the unit sphere by the relation

$$\mathbf{n} = \frac{\mathbf{q}}{|\mathbf{q}|}.$$



(a) The non-normalized vector \mathbf{q} lives on the ellipsoid.

(b) The Jeffery orbits arise from projecting \mathbf{q} on the unit sphere.

Figure 3.6: The Jeffery dynamics are simple on the ellipsoid inscribed in the unit sphere. The complicated non-linear orbits are recovered by projecting out to the unit sphere. The angles (γ, η) in the ellipsoid coordinates are the analogues of (θ, φ) on the unit sphere.

Using ellipsoidal and spherical parametrisations, respectively

$$\begin{cases} q_x = \sin \gamma \cos \eta \\ q_y = \frac{1}{\lambda} \sin \gamma \sin \eta \\ q_z = \cos \gamma \end{cases} \quad \begin{cases} n_x = \sin \theta \cos \varphi \\ n_y = \sin \theta \sin \varphi \\ n_z = \cos \theta \end{cases}$$

To find expressions for the spherical angles (θ, φ) we first note that

$$\frac{q_y}{q_x} = \frac{n_y}{n_x} \iff \frac{1}{\lambda} \tan \eta = \tan \varphi$$

and further

$$\frac{q_x^2 + q_y^2}{q_z^2} = \frac{n_x^2 + n_y^2}{n_z^2} \iff \tan^2 \gamma (\cos^2 \eta + \frac{1}{\lambda^2} \sin^2 \eta) = \tan^2 \theta$$

which after a slight rearrangement can be compared to the Jeffery equations (2.7) in section 2.4.

$$\begin{aligned} \tan \varphi &= \frac{1}{\lambda} \tan \eta \\ \tan \theta &= \frac{1}{\lambda} \tan \gamma \sqrt{\lambda^2 \cos^2 \eta + \sin^2 \eta} \\ \eta &= -\omega t = \frac{\sqrt{\alpha^2 + \beta^2} \lambda}{1 + \lambda^2} t \end{aligned}$$

3.3. DYNAMICS OF AXISYMMETRIC PARTICLES

Thus we have recovered the Jeffery orbits in a geometrically intuitive way. Moreover we can relate the unknown constant C in Jeffery's equations with our angle γ and the particle aspect ratio λ by

$$C = \frac{\tan \gamma}{\lambda}.$$

The period of the particle motion is directly related to the magnitude of the imaginary eigenvalue of the B -matrix, as

$$T = \frac{2\pi}{\omega}.$$

3.3.3 Experimental data

When we now turn back to the experimental observations, we want to see if the Jeffery theory is applicable. With the current theory and measurement technique only a qualitative comparison is possible. For a quantitative fit we would need to know the flow profile and the particle's position therein in great detail. An elaboration on why this is the case can be found in appendix A.2.

We can ask if there exists any Jeffery orbit that could explain the observed flips. This amounts to choosing

- a vorticity direction, that is alignment of the B -matrix eigenvectors,
- a shear strength, corresponding to the magnitude of the imaginary eigenvalue ω ,
- an effective particle aspect ratio λ ,
- the Jeffery orbit γ , and
- an initial condition η_0 .

Knowing more about the flow and particle position puts constraints on the first two items, defining the fundamental matrix. The effective particle aspect ratio really has to be matched this way since no real particle is a perfect ellipsoid, as explained by Bretherton [15]. For rod or cylinder like particles it will have to be close to the observed aspect ratio. The initial condition η_0 is just a phase shift for the fit, it does not change the characteristics of the motion.

A correction has to be made for the time scale. The theory is derived under the assumption that the shear strength is constant. In the measurements it fluctuates more than 25 %. The solution to this is a change of variables from time to distance along channel. By definition this makes the flow speed equal to unity (dimensionless) and the shear has units of m^{-1} instead of s^{-1} and the period "time" has units of distance. All plots in this report are thus plotted with distance along channel on the \hat{x} -axis. Because the Stokes equations are time independent, and the dynamics are inertialess this change of variables does not change the qualitative dynamics and the reader can simply think of the horizontal axis as time.

3.3. DYNAMICS OF AXISYMMETRIC PARTICLES

Two movies have been analyzed and fitted to the theory. We will refer to them simply as movie one and movie two. The first movie is shown in figure 3.7. Two different ways of visualizing the data are used. The sphere shows the trajectory in space of the unit vector \mathbf{n} attached to the particle. As the particle turns the tip of the vector traces a path on the sphere. This plot does not contain any temporal information and corresponds to fitting the vorticity direction and orbit constant only. We can see there exists a Jeffery orbit which fits the apparent trajectory of the particle for the duration of the movie. Fitting one trip from the north pole to the south is very easy with two parameters, but matching three consecutive flips is not an obvious result.

To see the effect of shear strength and initial condition we project the unit vector on the three cartesian axes and plot as a function of time. This is what is shown in the lower part of figure 3.7. This plot confirms the spatial fit of three consecutive flips. There is a slight change of time between the flips, less than 5 %.

The second movie is shown in figure 3.8. It shows three flips. There exists a Jeffery orbit which describes the orientation for the first two flips, and the period time for all three within a few percent. The last flip seems off, but it turns out that by only changing the orbit constant γ also the third flip is very well described. We interpret this as *drift between orbits*. Remember that according to Jeffery the orbit is decided by initial condition only, therefore we are observing another mechanism here.

Recall the infinite aspect ratio model by Turitsyn described in section 2.4.3. It predicts aperiodic flipping driven by stochastic forces. In contrast we seem to observe Jeffery-like periodic flips. Moreover the directions of the flips, that is the trajectories on the sphere, are not entirely random. It seems the observed dynamics are closer to Jeffery than to Turitsyn, but still neither is a perfect match.

Orbit drift aside, a feature not explained is the duration of the second flip. This mismatch is somewhat subtle. According to theory, all flips should be equally fast. In fact, for a fixed aspect ratio λ , the period time and flip duration are matched with only one parameter: the shear strength. The deviations manifest themselves as changes in peak widths in the time plot.

3.3.4 Possible perturbations

In this section we will briefly reason about possible causes for the observed deviations from theoretical predictions. In any experiment there will be noise, of course. But “noise” is a loose terminology, and we will discuss the two main suspected mechanisms for deviations from a deterministic Jeffery theory. No conclusive quantitative work has been done on the following points, but they serve as a guide for the future direction of this research.

Random fluctuations

Either thermal noise or fluctuations in the fluid flow profile can produce a stochastic force on the particle. In case of thermal fluctuations it is safe to assume that they are isotropic, which means independent of particle orientation. Flow fluctuations on the

3.3. DYNAMICS OF AXISYMMETRIC PARTICLES

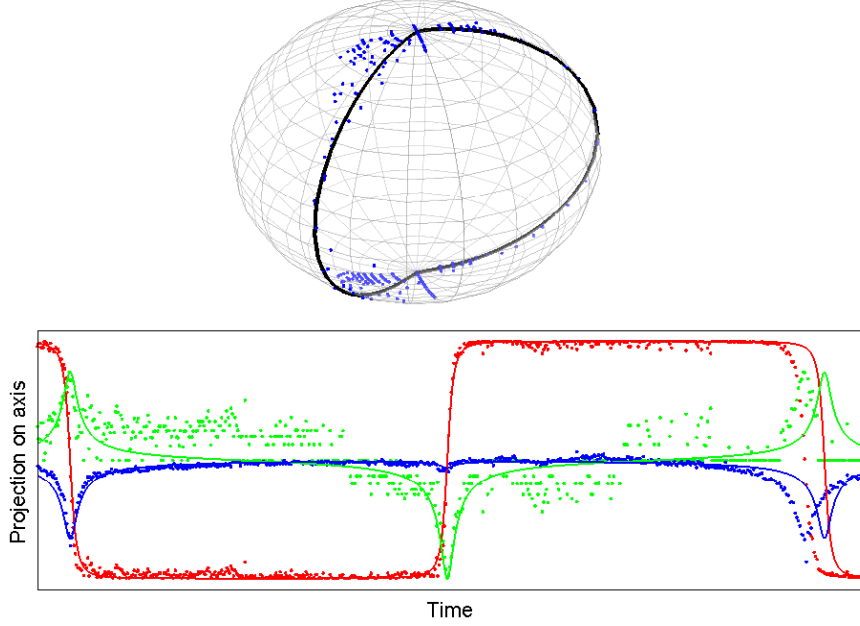


Figure 3.7: Movie 1. Experimental data and model fit. Top shows the unit sphere with the Jeffery orbit. Bottom shows time series of the direction vector projected onto the three coordinate axes.

other hand may well be anisotropic, stronger in one direction than another. In our rotation matrix formulation the random force amounts to an additive stochastic term in the equation of motion:

$$\frac{dR}{dt} = RQ(R) + \underbrace{W}_{\text{Noise}} \quad (3.11)$$

If the noise is anisotropic, W will depend on R . There is a dimensionless number called the Peclét number which is defined as

$$\text{Pe} = \frac{\alpha}{D_0}$$

where α is the shear strength and D_0 the noise strength. A large Peclét number means flow-dominated dynamics and a low number means noise-dominated dynamics. We numerically integrate (3.11) for different Peclét numbers in the case of isotropic noise. Typical resulting trajectories are shown in figure 3.9. We observe that when Peclét numbers decrease below a certain threshold, there is orbit drift, much like in our experimental observation. Very small Peclét number noise completely destroys the Jeffery periodicity.

3.3. DYNAMICS OF AXISYMMETRIC PARTICLES

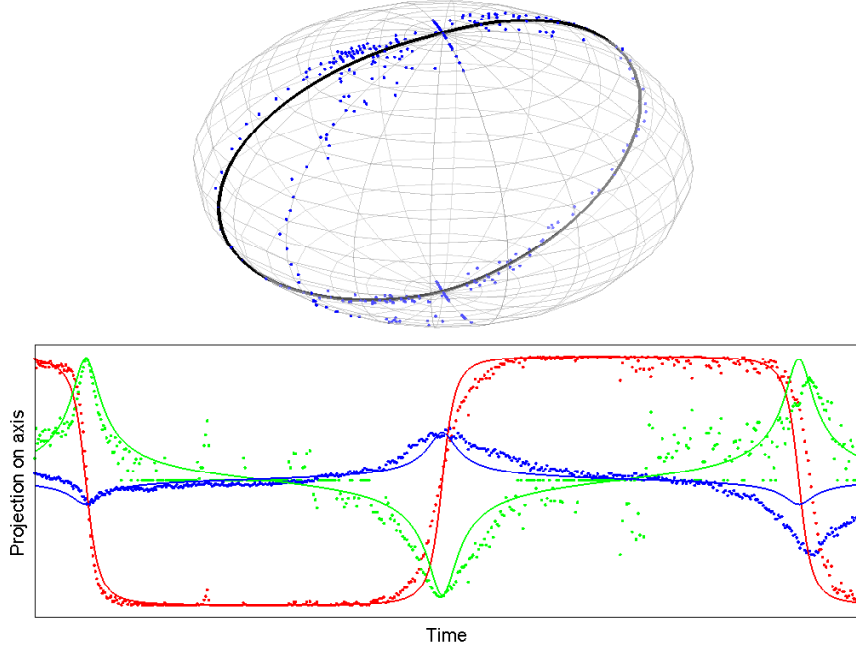


Figure 3.8: Movie 2. Experiment and model fit. Top shows the unit sphere with the Jeffery orbit. Bottom shows time series of the direction vector projected onto the three coordinate axes.

Asymmetry of particles

The specific case considered in this report was that of axisymmetric particles. A valid question is how sensitive the dynamics are to perturbations in this assumption. Yarim et al [23] published an analysis of the rotation of tri-axial particles under the Jeffery equations. They demonstrated that the dynamics become chaotic under certain circumstances. We numerically integrated the equation of motion using a triaxial particle with axis lengths $1:\varepsilon:10$. Typical resulting orbits are found in figure 3.10. As the asymmetry is increased the trajectories become more and more dispersed. Even for small asymmetries ($\varepsilon = 2$) it is found that the dynamics escape the Jeffery orbits.

3.3. DYNAMICS OF AXISYMMETRIC PARTICLES

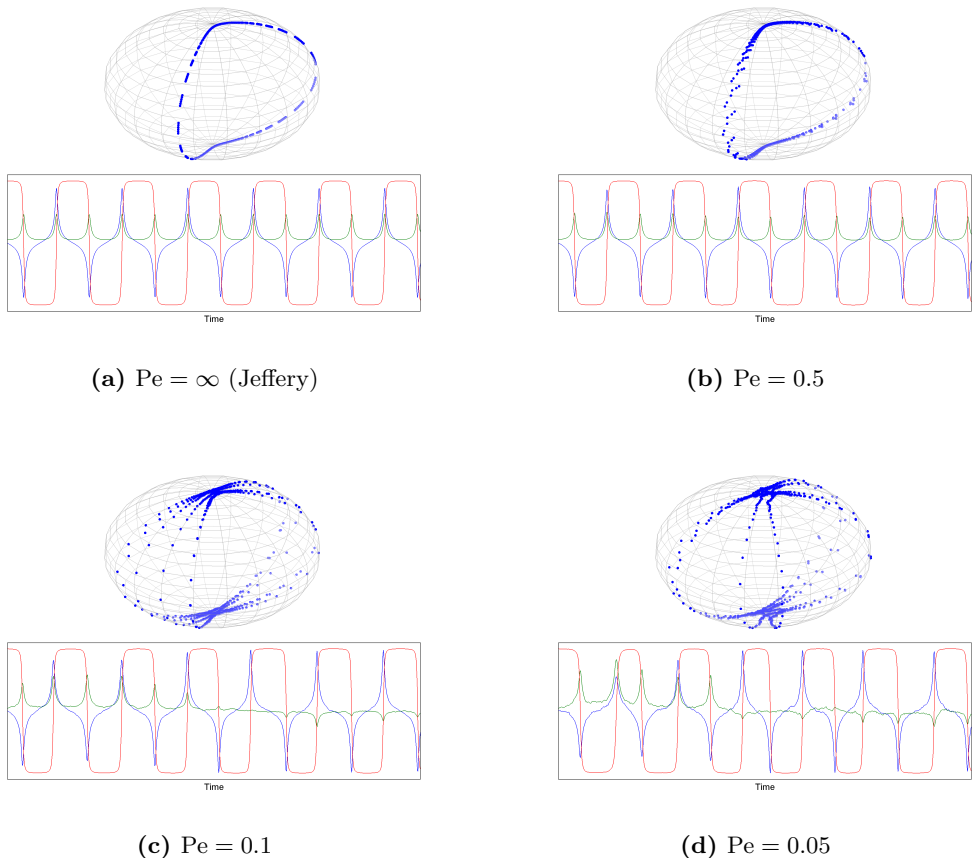


Figure 3.9: Numerical integration of noisy equation of motion. The noise is isotropic and noise strength increases from left to right and top to bottom as indicated by Peclét numbers. When Peclét numbers decrease below a certain threshold, there is orbit drift. Very small Peclét number noise completely destroys the Jeffery periodicity.

3.3. DYNAMICS OF AXISYMMETRIC PARTICLES

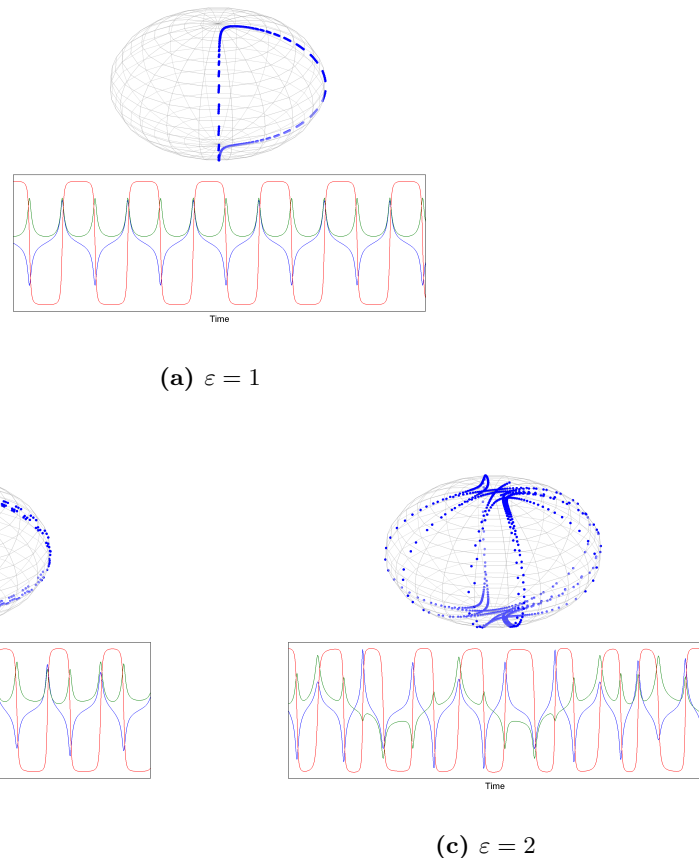


Figure 3.10: Numerical integration of equation of motion with a triaxial particle. The axis lengths are $1:\varepsilon:10$. $\varepsilon = 1$ corresponds to regular Jeffery motion. As the asymmetry is increased the trajectories become more and more dispersed. Even for small asymmetries ($\varepsilon = 2$) it is found that the dynamics escape the Jeffery orbits.

3.4 Conclusions & Outlook

Where are we now, and where are we heading? From the current experimental observations we stand fairly convinced that the Jeffery model has real significance in some systems. We have also seen contradictions to a pure Jeffery world. We would like to conclude this report with a few comments on how to further develop our understanding, relating to both the experimental as well as the theoretical side.

3.4.1 Experiments

As elaborated on in appendix A.2 there are a number of unknowns in the current experimental setup. The experiments evolved from microchannel experiments on biological systems where the exact flow profile was not important. Equipped with the new knowledge and experience documented in this report we can make a few suggestions. Let us make a wish list from a theorist's perspective, we would like experiments that

- observe all degrees of freedom of an individual particle,
- for an extended period of time,
- in a known, uniform and linear flow.

In reality this would for example require two cameras observing the same particle at all times. It is not easily done. Manufacturing microchannels to arbitrary dimensions is also non-trivial. For practical purposes we suggest the following two setups:

1. Build microchannels of much wider aspect ratio. Then the flow near the middle of the channel is basically a shear flow with a known vorticity direction. This would remove one fit parameter directly. It would also facilitate measurements of the flow profile with particles or by volumetric flow. In a perfect world we would also observe the particle from the known vorticity direction, but this might be very difficult in practise.
2. Build a microfluidic device corresponding to a circular Taylor-Couette flow, generating a vortex. A sketch of the microfluidic layout is in figure 3.11. If a particle is trapped in a closed vortex loop it could be observed for long times. The vorticity direction would also be known, and pointing towards the camera. However, measuring the exact flow profile might prove more difficult than in a straight channel.

The first one is doable with current equipment, today. The second suggestion requires some calculation of dimensions and trials to see what the actual flow profile looks like, but the manufacturing technique could be the same.

3.4.2 Theory

The observed deviations from Jeffery orbits tells us to look for other mechanisms. In the previous section we saw that isotropic noise can account for orbit drift without affecting

3.4. CONCLUSIONS & OUTLOOK

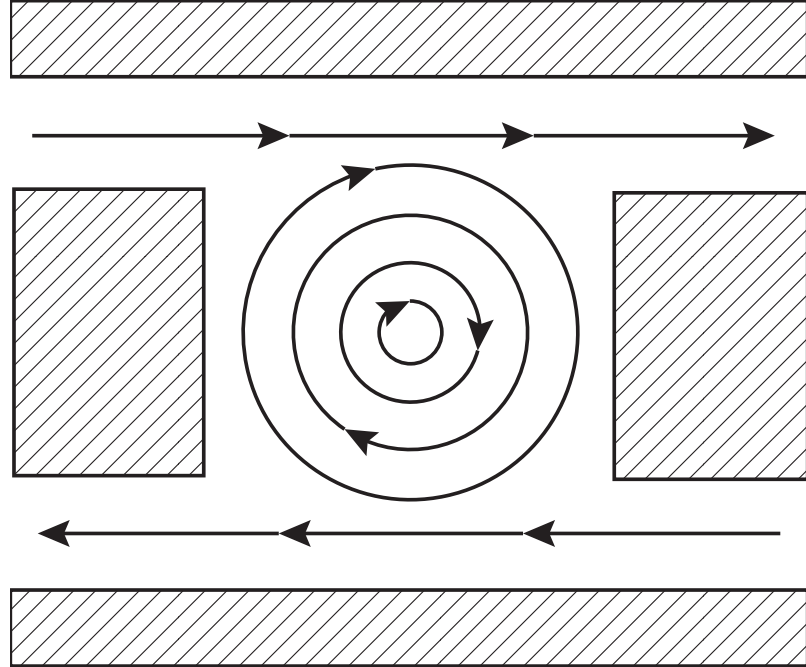


Figure 3.11: Suggestion for microfluidic device for generating a Couette-Taylor flow. In macroscopic experiments it is achieved with rotating, concentric cylinders. In microfluidics a vortex could be driven by friction from a pressure driven flow. The connections should be pressurized from top-left to top-right, and bottom-right to bottom-left.

the periodicity appreciably. Particle asymmetry seems to be a sensitive parameter, but the numerical results show a strong aperiodicity which we have no experimental observation of.

The Turitsyn approach is based entirely on isotropic noise, but its predictions do not match our experimental data either. We hypothesize that there is a phase diagram of these complementary theories. There is a low-noise, finite aspect ratio region as well as a infinite aspect ratio, high-noise region. A sketch is found in figure 3.12. The coming task is to map out this phase diagram numerically, using the framework we developed in this thesis. One question is for example what infinite aspect ratio means in practise? Is it 25, 100 or 1000? Does it even occur, or does every real system have some Jeffery behavior?

With our main equation for the rotation matrix R including noise W

$$\frac{dR}{dt} = RQ + W$$

we have the tool to map out lines in the phase diagram, and look for transitions to noise-driven dynamics.

3.4. CONCLUSIONS & OUTLOOK

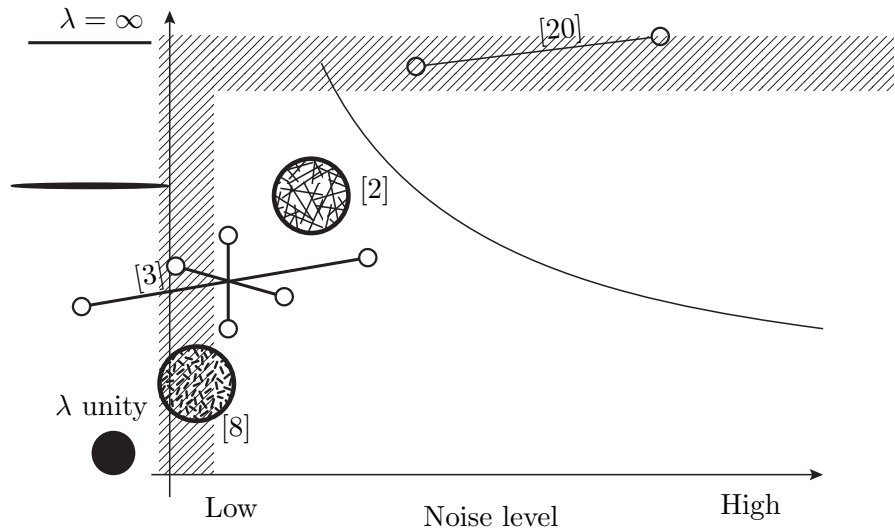


Figure 3.12: Proposed phase diagram over theories of particle motion. To the left are deterministic, or low-noise, models dominated by Jeffery type behavior. In this regime the main forces are typically hydrodynamic. To the right are Turitsyn-like noise-driven dynamics. Vertical axis shows aspect ratio, varying from spherical particles at the bottom, to rods at the top. Our hypothesis is that the sensitivity to noise is dependent on aspect ratio, and that high aspect ratio particles are more sensitive to perturbation. The experiments discussed in this report are most likely situated somewhere near the Jeffery limit, but in the finite noise region. References in figure correspond to theories by Jeffery [3], Turitsyn [20] and experiments by Kaya, Koser [8]; Oladiran, Hanstorp [2].

Bibliography

- [1] A. Einstein, Eine neue bestimmung der moleküldimensionen, Annalen der Physik 324 (2) (1906) 289–306.
- [2] A. Oladiran, Microrod movements in a microfluidic system, M.Sc Thesis, Unpublished.
- [3] G. Jeffery, The motion of ellipsoidal particles immersed in a viscous fluid, Proceedings of the Royal Society of London. Series A 102 (715) (1922) 161–179.
URL <http://www.jstor.org/stable/94111>
- [4] V. Bezuglyy, B. Mehlig, M. Wilkinson, Poincare Indices of Rheoscopic Visualisations (2009) 4.
URL <http://arxiv.org/abs/0903.3615>
- [5] M. Wilkinson, V. Bezuglyy, B. Mehlig, Emergent order in rheoscopic swirls, Journal of Fluid Mechanics (2010) 1–30.
URL http://www.journals.cambridge.org/abstract_S0022112010004441
- [6] M. Wilkinson, V. Bezuglyy, B. Mehlig, Fingerprints of random flows?, Physics of Fluids 21 (4) (2009) 043304.
URL <http://link.aip.org/link/?PHF/21/043304/1>
- [7] D. E. Smith, H. P. Babcock, S. Chu, Single-Polymer Dynamics in Steady Shear Flow, Science 283 (5408) (1999) 1724–1727.
URL <http://www.sciencemag.org/content/283/5408/1724.abstract>
- [8] T. Kaya, H. Koser, Characterization of Hydrodynamic Surface Interactions of Escherichia coli Cell Bodies in Shear Flow, Physical Review Letters 103 (13) (2009) 1–4.
URL <http://link.aps.org/doi/10.1103/PhysRevLett.103.138103>
- [9] P. Kundu, I. Cohen, Fluid Mechanics, Elsevier Academic Press, 2004.

BIBLIOGRAPHY

- [10] J. Happel, H. Brenner, Low Reynolds number hydrodynamics: with special applications to particulate media, Kluwer Academic Print on Demand, 1991.
- [11] S. Kim, S. Karrila, Microhydrodynamics: principles and selected applications, Vol. 507, Butterworth-Heinemann Boston, 1991.
- [12] F. Morrison, What is rheology anyway, online on The Industrial Physicist at: www.aip.org/tip/INPHFA 10.
- [13] A. Oberbeck, Ueber stationäre Flüssigkeitsbewegungen mit Berücksichtigung der inneren Reibung., Journal für die reine und angewandte Mathematik (Crelle's Journal) 1876 (81) (1876) 62–80.
- [14] E. Hinch, L. Leal, Rotation of small non-axisymmetric particles in a simple shear flow, Journal of Fluid Mechanics 92 (03) (1979) 591–607.
- [15] F. Bretherton, The motion of rigid particles in a shear flow at low Reynolds number, Journal of Fluid Mechanics 14 (02) (1962) 284–304.
- [16] R. Eisenschitz, Die Viskosität von Suspensionen langgestreckter Teilchen und ihre Interpretation durch Raumbeanspruchungen, Z. phys. Chem. A 158 (1931) 78.
- [17] L. Leal, E. Hinch, Theoretical studies of a suspension of rigid particles affected by Brownian couples, Rheologica Acta 12 (2) (1973) 127–132.
URL <http://www.springerlink.com/index/j8737514t48085n7.pdf>
- [18] E. Hinch, L. Leal, The effect of Brownian motion on the rheological properties of a suspension of non-spherical particles, Journal of Fluid Mechanics 52 (04) (1972) 683–712.
URL http://journals.cambridge.org/abstract_S002211207200271X
- [19] M. Rahnama, D. L. Koch, E. S. G. Shaqfeh, The effect of hydrodynamic interactions on the orientation in a fiber suspension subject to simple shear flow distribution, Physics of Fluids 7 (3) (1995) 487–506.
- [20] K. Turitsyn, Polymer dynamics in chaotic flows with a strong shear component, Journal of Experimental and Theoretical Physics 105 (2007) 655–664, 10.1134/S1063776107090245.
URL <http://dx.doi.org/10.1134/S1063776107090245>
- [21] R. Bird, R. Armstrong, O. Hassager, Dynamics of polymeric liquids, John Wiley and Sons Inc., New York, NY, 1987.
- [22] A. Szeri, Pattern formation in recirculating flows of suspensions of orientable particles, Philosophical Transactions of the Royal Society of London A 345 (1677) (1993) 477.

BIBLIOGRAPHY

- [23] A. Yarin, O. Gottlieb, I. Roisman, Chaotic rotation of triaxial ellipsoids in simple shear flow, *Journal of Fluid Mechanics* 340 (1997) 83–100.
URL http://journals.cambridge.org/abstract_S0022112097005260
- [24] G. Folland, Fourier analysis and its applications, Amer Mathematical Society, 2009.

A

Calculations & notes

A.1 Numerically integrating SO(3)

Our equation of motion is defined for a rotation matrix R :

$$\frac{dR}{dt} = RQ, \quad (\text{A.1})$$

where Q is an skew-symmetric matrix. The problem of integrating three dimensional rotations is not new. The basic problem is that there exists no smooth mapping from the rotation group to \mathbf{R}^3 . For practical purposes there exists several ways to parametrize rotations, from the infamous singular Euler angles to using unit quaternions. We have used rotation matrices which actually have 9 real numbers to represent a three dimensional rotation. The group of matrices that represent the rotation group in three dimensions is called SO(3). To represent an element in SO(3) with a matrix R the following two constraints must hold for R :

$$R^T R = R R^T = 1$$

$$\det R = 1$$

If we naively integrate equation (A.1) it will violate these constraints due to numerical error. The key for our scheme is to realize that every skew-symmetric matrix Q is a *generator* of a rotation. More precisely they can be written as linear combinations of the three fundamental generators of SO(3). Using this “basis” (I_1, I_3, I_3) of generators for rotations, any rotation R can be written as

$$R = \exp(aI_1 + bI_3 + cI_3)$$

with a, b, c arbitrary scalars. Make the change of variables

$$R = \exp(\Psi)$$

A.1. NUMERICALLY INTEGRATING $SO(3)$

which transforms equation (A.1) to

$$\frac{d\Psi}{dt} = Q.$$

In this generator space there are only three degrees of freedom, the coefficients for the three fundamental generators, which can be integrated using any convenient numerical scheme on \mathbf{R}^3 . Then $R(t)$ should be given by

$$R(t) = \exp(\Psi(0) + \int_0^t Q(t)dt)$$

However, this does not work because the rotations described by Q can be degenerate. Think of Q as describing an axis of rotation and an angle. Then for any axis the rotation of angle 2π is the same. More subtly, the rotation of π through one axis is the same as rotation $-\pi$ about another. In theory the scheme works for angles up to $|\theta| < \pi$. In reality the integration only has good numerical precision for small deviations from the identity rotation. The solution we used is to take a small time step and then make a change of variables to the identity rotation again. Given an initial condition R_0 the algorithm does the following. Start with

$$R(t) = r(t)R_0, \quad r(0) = 1$$

which gives an equation for r of form (A.1) but with initial condition equal to the identity rotation:

$$\frac{dr}{dt} = rR_0Q(t)R_0^{-1}$$

This equation is integrated for a small timestep Δt

$$r(\Delta t) = \exp\left(\int_0^{\Delta t} R_0Q(t)R_0^{-1}dt\right)$$

where we used the fact that Ψ_0 is zero for the identity initial condition, guaranteeing the exponential argument to be small. Now we reset the initial condition by

$$R_1 = r(\Delta t)R_0,$$

and repeat the procedure with R_1 in place of R_0

$$R(\Delta t + t) = r(t)R_1, \quad r(0) = 1.$$

This is the scheme which has been used for generating all numerical results presented in this report.

A.2 On the experimental fit

When comparing the experiments to the theory we did some hand-waving and argued that only a qualitative comparison was feasible. Here we will elaborate briefly on why. If we knew perfectly the undisturbed flow in the channel, and the particle's position therein, we could in principle predict the resulting trajectory without any parameters. However, since the particle is not a perfect ellipsoid it will have an effective aspect ratio [15] which could vary slightly from the measured value. For now we will say that we can measure the particle aspect ratio, it does not affect the following in any serious way.

A.2.1 The method used

In addition to the slight uncertainty in particle aspect ratio we cannot, in the current experiments, measure:

- The particle \hat{y} (depth) coordinate,
- The local flow shear direction at the particle, nor
- shear strength.

Let's first consider matching a trajectory with a Jeffery orbit without the temporal information. That amounts to specifying alignment of the B -matrix eigensystem, and an orbit constant γ . The former is dependent on the local shear direction of the flow. Since our microchannel has finite aspect ratio it will vary with both \hat{x} (side-to-side) and \hat{y} (depth) coordinate of the particle. The orbit constant γ is an observable given by any point on the trajectory, or conversely, every point on the observed trajectory corresponds to some γ . We want to know if there is a single γ to fit all points.

So far only one arbitrary parameter, the flow shear direction. When we proceed to match a trajectory also in the time domain, we have to specify a flow shear strength. This effectively specifies the magnitude of the imaginary eigenvalue of the B -matrix. Using this and an initial condition η_0 we can fit the period of the orbit previously matched.

These two preceding paragraphs described how we first could match the spatial trajectory with two parameters and then, independently, the temporal characteristics with another parameter. With that many degrees of freedom it is no surprise if we can match any trajectory closely. The only things that makes this fit worth anything is that it matches several consecutive flips, and that it is periodic within a few percent.

A.2.2 Attempt of improvement

The problem is that we choose the eigensystem of the B -matrix freely and therefore can match spatial and temporal information independent parameters. If we knew more about the flow, it would put constraints on the B -matrix. By solving the Stokes equations for a pressure driven channel flow we know the theoretical non-linear flow field up to a

A.2. ON THE EXPERIMENTAL FIT

constant k as

$$\mathbf{u}(x,y) = \sum_{l=0}^{\infty} \frac{2k(-1)^l}{w\lambda_l^3} \left(1 - \frac{\cosh \lambda_l y}{\cosh \lambda_l h} \right) \cos(\lambda_l x) \hat{\mathbf{z}}, \quad \lambda_l = \frac{\pi}{w} \left(l + \frac{1}{2} \right) \quad (\text{A.2})$$

where now (x,y) are the side-to-side and depth coordinates, respectively, of the particle. w and h is the width and depth of the channel. The flow is along the channel, which is the $\hat{\mathbf{z}}$ -direction. The derivation of this expression is found in appendix A.3. From the movies we can measure the x -coordinate, and we know the channel width and height from specifications. Assuming that the particle is advected perfectly, we know the flow speed at the particle. Using that we can solve (A.2) for either the y -coordinate or the constant k .

Say that we use the depth y -coordinate as free parameter. Then the flow, and by extension the B -matrix is known. That leaves only the orbit constant γ and η_0 as parameters, which is the same as choosing an initial condition. Trying this for the second movie, using the y -coordinate as a free parameter yields a fit like figure A.1. But for

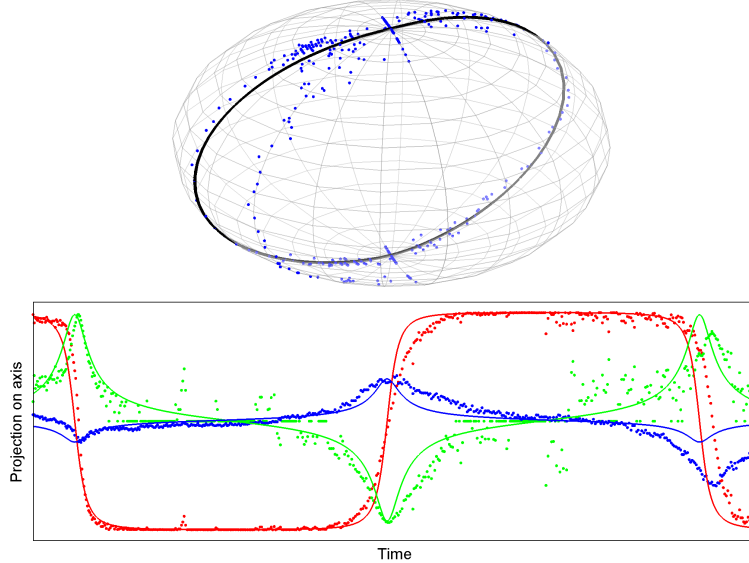


Figure A.1: Experimental fit for the second movie using analytical flow model. With fixed aspect ratio, the only free parameters are the y -coordinate (depth) and an initial condition.

the first movie, there is no depth which gives a fit using any reasonable particle aspect ratio λ . To understand why, let's take a closer look at the flow profile described by equation (A.2). In figure A.2 we show the contour lines of the flow, contour lines of the shear strength and contour lines of the angle of the vorticity direction. The two latter

A.2. ON THE EXPERIMENTAL FIT

describes the flow gradient and thus the B -matrix. The two experiments are annotated with vertical lines. Movie 2, which was possible to fit, has a reasonable sensitivity between angle and shear strength. Closer to the middle of the channel, where movie 1 is, the angle is extremely dependent on shear strength. That is why there is no single match. Of course a real flow deviates from this theoretical model enough to make this kind of sensitivity ridiculous.

To use the flow in quantitative matches a future experiment should have a simpler profile which can be measured to calibrate an appropriate theoretical model. For example by making the channel very much wider and only observing a small part in the middle would make the vorticity direction same everywhere in the observed part of the channel.

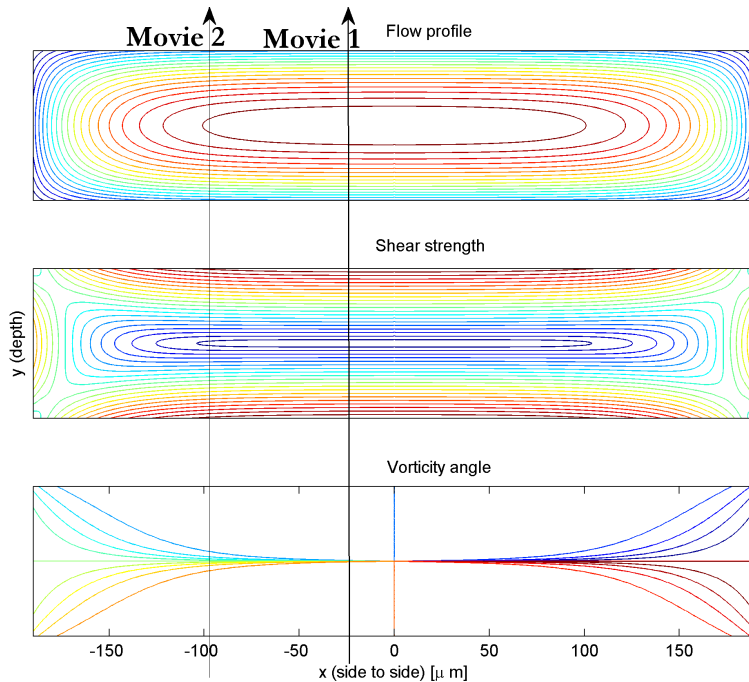


Figure A.2: Analytical solution of the flow profile in our microchannel. Top shows contour lines for the flow. Middle shows shear strength and bottom shows angle from vorticity axis to the x -axis. Two vertical lines mark where the particle is in the two analyzed experiments. Movie two is possible to fit with one parameter, but for movie one there is no matching angle and shear strength.

A.3 Pressure driven flow in rectangular channel

In channel flow we assume the flow to be only in the **z**-direction. Then the Stokes equations with no slip boundary conditions are

$$(\frac{\partial^2}{\partial x^2} + \frac{\partial^2}{\partial y^2})u_z(x,y) = -\frac{P}{\eta} \equiv -k \quad (\text{A.3})$$

with

$$\begin{aligned} u(-w,y) &= 0 \\ u(w,y) &= 0 \\ u(x,-h) &= 0 \\ u(x,h) &= 0 \end{aligned} \quad (\text{A.4})$$

This Poisson equation is solvable by separation of variables as follows [24]. Assume $u_z(x,y) = f(x)g(y)$, then the homogenous part of (A.3) separates into two ordinary differential equations

$$\begin{aligned} f'' + \lambda^2 f &= 0 \\ g'' - \lambda^2 g &= 0 \end{aligned}$$

with λ an arbitrary complex constant. The equation for $f(x)$ is solved with boundary conditions (A.4) to

$$f_l(x) = C_l \cos(\lambda_l x), \quad \lambda_l = \frac{\pi}{w}(n + \frac{1}{2}), \quad l = 0, 1, 2, \dots$$

We have a basis in x , and we can write the total flow function as a linear superposition

$$u_z(x,y) = \sum_{l=0}^{\infty} g_l(y) \cos(\lambda_l x) \quad (\text{A.5})$$

this expression is back-substituted directly into the Stokes equation (A.3) which yields

$$-\sum_{l=0}^{\infty} g_l(y) \lambda_l^2 \cos(\lambda_l x) + \sum_{l=0}^{\infty} g_l''(y) \cos(\lambda_l x) = -k$$

Multiplying with $\cos(\lambda_l x)$ and integrating over x eliminates the sum and we get an ordinary inhomogenous differential equation for $g_l(y)$:

$$g_l''(y) - \lambda_l^2 g_l(y) = -\frac{2k(-1)^l}{w\lambda_l}$$

which is in turn solved, taking the boundary conditions (A.4) into account, by

$$g_l(y) = \frac{2k(-1)^l}{w\lambda_l^3} \left(1 - \frac{\cosh \lambda_l y}{\cosh \lambda_l h} \right)$$

A.3. PRESSURE DRIVEN FLOW IN RECTANGULAR CHANNEL

The final result is obtained by insertion in (A.5) which yields

$$u_z(x,y) = \sum_{l=0}^{\infty} \frac{2k(-1)^l}{w\lambda_l^3} \left(1 - \frac{\cosh \lambda_l y}{\cosh \lambda_l h} \right) \cos(\lambda_l x) \quad (\text{A.6})$$